Quaternary Science Reviews 391 (2026) 110236

Contents lists available at ScienceDirect

Quaternary Science Reviews

journal homepage: www.elsevier.com/locate/quascirev

Paleovalley fills as terrestrial archives of Mediterranean Sapropel S1: insights from the Biferno Paleovalley System (Southern Italy)

B. Campo [a,*], A. Di Martino [a], A. Nogarotto [b], F. Purri [a], V. Rossi [a], T. Tesi [b], S.C. Vaiani [a], W. Hong [c], I.A. De Vincenzo [a], C. Pellegrini [d,1], A. Amorosi [a,1]

[a] Dipartimento di Scienze Biologiche, Geologiche e Ambientali (BiGeA), Università di Bologna, Piazza di Porta San Donato 1, Bologna, 40126, Italy
[b] Istituto di Scienze Polari - Consiglio Nazionale delle Ricerche ISP-CNR, Bologna, Italy
[c] KIGAM Korea Institute of Geoscience and Mineral Resources, 92 Gwahangro, Yuseong-gu, Daejeon Metropolitan City, South Korea
[d] Consiglio Nazionale delle Ricerche (CNR), Istituto di Scienze Marine (ISMAR), Via Roberto Cozzi 53, Milano, 20125, Italy

ARTICLE INFO

Handling Editor: Dr Mira Matthews

Keywords:
Paleovalley systems
Source-to-sink
Sapropel S1-equivalent succession
Onshore-offshore correlation
Adriatic sea

ABSTRACT

Sapropel S1 corresponds to the latest deoxygenation event that occurred in the Mediterranean Sea between ~10.2 and 6.8 cal kyr BP. However, terrestrial deposition coeval with Mediterranean Sapropel S1 remains poorly understood. Through the integration of sedimentological, paleontological, geochemical (TOC, TN, $\delta^{13}C$, $\delta^{15}N$) and chronological data within a regional onshore-offshore framework, this study investigates the Upper Pleistocene-Holocene fill of the Biferno paleovalley system (Southern Italy) and characterizes the S1-equivalent ($S1_{eq}$) succession.

The results document a continuous $S1_{eq}$ record comprising three stratigraphic intervals ($S1a_{eq}$, $S1break_{eq}$, and $S1b_{eq}$) that can be correlated with the corresponding offshore S1 phases. Facies evolution from poorly-drained floodplain to estuarine deposits reflects Holocene relative sea-level rise and paleovalley drowning. Bulk geochemical proxies display strong stratigraphic control, with $\delta^{13}C$ and $\delta^{15}N$ trends closely tracking facies shifts and Organic Matter (OM) sources.

Onshore-offshore correlation and comparison with other Adriatic paleovalley systems reveal a marked decoupling in organic-carbon accumulation during the S1 break, consistent with the progressive landward migration of river mouths during the Holocene transgression. This evolution promoted enhanced terrigenous OM storage within paleovalleys while reducing its export toward deeper basin sectors.

These findings indicate that paleovalley systems constitute key transient repositories of sediment and organic carbon during rapid transgression and provide a valuable terrestrial archive for reconstructing the evolution of the Adriatic source-to-sink system during Mediterranean Sapropel S1 deposition. Their stratigraphic record offers a critical link between continental and marine systems, providing new constraints on the environmental processes accompanying S1 deposition in the Adriatic and Mediterranean regions.

1. Introduction

Paleovalley systems (PVSs; *sensu* Blum and Törnqvist, 2000) are fundamental archives of the Quaternary stratigraphic record (Allen and Posamentier, 1993; Bhattacharya, 2011; Boyd et al., 2006; Dalrymple, 2006; Legarreta and Uliana, 1998; Shanley and McCabe, 1991, 1992; Wright and Marriott, 1993), and have been widely recognized as key geomorphic and stratigraphic elements formed primarily during phases of relative sea-level fall (Posamentier and Vail, 1988; Posamentier et al., 1988; Van Wagoner et al., 1988, 1990). Late Quaternary PVSs, in particular, provide exceptional opportunities to investigate the coupling between climate, sea-level change, and sediment routing, as their development occurred during well-constrained glacial-interglacial cycles and their deposits can be robustly dated and correlated (Blum et al., 2013). Experimental and numerical studies (Strong and Paola, 2006, 2008) confirmed that relative sea-level fall represents the primary control on valley incision, driving fluvial erosion through older coastal and shelf deposits, while channel-belt migration and deposition shaped

* Corresponding author.
E-mail address: bruno.campo@unibo.it (B. Campo).
[1] These authors contributed equally as senior authors.

https://doi.org/10.1016/j.quascirev.2026.110236
Received 1 April 2026; Received in revised form 15 August 2026; Accepted 15 August 2026
Available online 21 August 2026
0277-3791/© 2026 The Authors. Published by Elsevier Ltd. This is an open access article under the CC BY license (http://creativecommons.org/licenses/by/4.0/).

valley morphology during subsequent lowstand conditions (Holbrook et al., 2006). Subsequent phases of sea-level rise and highstand provoked the gradual filling of PVSs (Zaitlin et al., 1994). Owing to enhanced accommodation potential compared to interfluves (Wang et al., 2019), late Quaternary paleovalley fills (PVFs) commonly preserve stratigraphically expanded successions, including falling-stage and lowstand deposits that are otherwise poorly recorded in coastal and shelf settings (Blum and Aslan, 2006; Lai et al., 2025; Rodriguez et al., 2005; Rossi et al., 2017; Simms et al., 2007; Tanabe et al., 2026; Thomas and Anderson, 1994). PVFs generally display a characteristic stratigraphic architecture, with basal amalgamated sand-gravel fluvial bodies overlain by finer-grained, mud-dominated successions containing more isolated ribbon- and sheet-like channel sands (Blum, 1993; Legarreta and Uliana, 1998; Li et al., 2002; Lin et al., 2005; Sakai et al., 2006; Shanley and McCabe, 1992, 1994; Sloss et al., 2010; Tanabe et al., 2006, 2013). This vertical organization reflects the combined influence of upstream boundary conditions (water supply, sediment supply, tectonics) and downstream controls imposed by relative sea-level changes (Blum et al., 2013). The investigation of PVFs can also provide insights into paleoclimate variations (Blum, 2007; Drago et al., 2006; Ishihara and Sugai, 2017; Peeters et al., 2015; Simms et al., 2010), and environmental changes caused by different allogenic or autogenic factors (Amorosi et al., 2009; Chaumillon et al., 2010; Durand et al., 2018; Horozal et al., 2021). Furthermore, recent studies have highlighted how PVFs induce abrupt shifts in resonance frequencies from the paleovalley flanks to the depocenter (Di Martino et al., 2024). Their geometry and sedimentary infill may also alter ground motion during earthquakes, leading to seismic amplification (Di Martino et al., 2024) and severe structural damage (Tanabe et al., 2015; Tanabe and Ishihara, 2021).

Beyond their stratigraphic significance, PVSs are fundamental components of source-to-sink (S2S) sediment-routing systems (Blum et al., 2013), governing sediment storage, transfer, and connectivity between continental catchments and marine depocenters (Goodbred et al., 2003; Sømme et al., 2009; Zhang et al., 2021). Coastal PVSs represent critical onshore nodes within basin-scale S2S systems, as demonstrated by the Golo system in the Mediterranean area (Sweet, 2020; Sømme et al., 2011). However, the role of PVSs in modulating basin-wide sedimentary and geochemical events remains mostly unexplored, especially in relation to large-scale paleoceanographic perturbations.

In the Mediterranean Sea, sapropels represent some of the most prominent expressions of Quaternary environmental changes, associated with periodic perturbations of marine ecology and geochemistry (Nijenhuis et al., 1996; Tesi et al., 2024). Sapropels were originally defined as organic-rich layers (>2 wt% TOC), generally thicker than 1 cm (Kidd et al., 1978), deposited during episodes of reduced bottom-water ventilation (Rogerson et al., 2008) and enhanced oceanic water stratification, commonly linked to periods of insolation minima and increased freshwater input (Hilgen, 1991; Rohling et al., 2015; Rossignol-Strick, 1985; Rossignol-Strick et al., 1982). These solar variations resulted in periodic intensification of the African monsoons which in turn increased freshwater input to the Eastern Mediterranean via the Nile River (Weldeab et al., 2014). Meanwhile, an increase in autumn-winter precipitation along the borderlands of the Mediterranean increased the runoff further reducing sea surface salinities and increasing the nutrient supply (Toucanne et al., 2015; Wagner et al., 2019). As a result, the freshening generated a wide-basin weakening of the thermohaline circulation and stimulated algal blooms sustained by nutrients (De Lange et al., 2008). The Adriatic Sea plays a first-order role in Eastern Mediterranean deep-water formation and ventilation (Klein et al., 2000), and continental freshwater runoff has been recognized as one of the key factors contributing to the formation of the latest sapropel S1 event (~10.2-6.8 cal kyr BP; De Lange et al., 2008; Hennekam et al., 2014; Schmiedl et al., 2010). Nevertheless, terrestrial deposits coeval with Mediterranean Sapropel S1 (hereafter referred to as sapropel-equivalent deposits) have received little attention. Although there is evidence that Adriatic S1 was driven by African monsoon (Schmiedl et al., 2010), little is known about the role of freshwater discharge from local rivers during S1 deposition. Furthermore, besides the Organic Matter (OM) delivered by terrestrial systems (soil-delivered OM, plant debris and riverine phytoplankton), primary production is closely tied to riverine and terrestrial dynamics as riverine plumes supply nutrients to marine phytoplankton (Tesi et al., 2007). Therefore, investigating coastal systems is essential for reconstructing land-sea interactions during S1 deposition.

Along the western Adriatic margin, the S1-equivalent is more likely to be preserved within PVFs, where up to 20 m thick organic-rich successions have been documented, whereas coeval deposits are generally absent or strongly condensed on the laterally extensive interfluve areas (Amorosi et al., 2016a, 2022; Campo et al., 2022; Fontana et al., 2008; Maselli and Trincardi, 2013; Ricci Lucchi et al., 2006; Ronchi et al., 2021). In this regard, previous work on the South Adriatic shelf proposed that the evolution of the Manfredonia paleovalley and the associated fluvio-deltaic system was controlled by climatic and sea-level changes accompanying Sapropel S1 deposition (Maselli et al., 2014). Accordingly, the spatially selective preservation of S1-equivalent successions suggests that PVSs may have played a previously overlooked role in mediating sediment, OM, and freshwater fluxes during Sapropel S1 deposition.

In this study, the Biferno PVS was investigated with the aim of identifying and characterizing the S1-equivalent stratigraphic intervals, shedding some light on the contribution of paleovalley systems to the deposition of S1 in the Adriatic Sea. A new sediment core (T1), recovered from the depocentral sector of the Biferno PVF to target a relatively continuous S1-equivalent succession, penetrated the Upper Pleistocene-Holocene succession preserved at the site, down to the underlying substrate. The core was investigated through integrated sedimentological, paleoecological (benthic foraminifers and ostracods), geochemical (TOC, TN, $\delta^{13}C$, $\delta^{15}N$), and chronological analyses. Results were framed within a basin-scale S2S context using published stratigraphic, seismic, pollen, and geochemical datasets from the western Adriatic Sea (Amorosi et al., 2016a, 2016b, 2021, 2022; Cacciari et al., 2020; Campo et al., 2024; Tesi et al., 2017). The objectives of this paper are to (i) reconstruct the Biferno PVF facies architecture, (ii) identify and characterize the onshore (terrestrial) equivalent of S1, and (iii) evaluate how coastal PVSs modulate sediment routing and preservation during major late Quaternary paleoenvironmental changes, with a focus on the S1 event.

2. Regional setting

2.1. The biferno coastal plain

The Biferno River is a ~93 km-long-fluvial system draining the northeastern flank of the central-southern Apennines and flowing eastward into the Adriatic Sea (Fig. 1a and b; Aucelli et al., 2009; Mancinelli et al., 2023). Its drainage basin covers approximately 1316 km^2 and originates at the foot of the Matese carbonate massif (Rosskopf and Scorpio, 2013). Marked climatic gradients across the basin exert a strong control on hydrological regime, characterized by pronounced seasonal variability typical of Apennine torrential systems. The Biferno coastal plain represents the distal sector of the river course, extending from the Ponteliscione dam to the Adriatic shoreline (Fig. 1c). Downstream of the dam, channel gradients decrease from ~0.68% to ~0.24%, while the valley floor progressively widens from 0.5 to 0.7 km to more than 2 km. This morphological transition is accompanied by a shift from a relatively confined channel to a sinuous-meandering planform, reflecting reduced stream power and enhanced lateral mobility (Rosskopf and Scorpio, 2013). The evolution of the Biferno valley has been influenced by long-term regional uplift and Quaternary tectonic activity, which promoted valley incision and the development of multiple fluvial terraces (Amato et al., 2017; Ferrarini et al., 2021; Mancinelli et al., 2023; Scrocca and Tozzi, 1999). In the distal valley, the

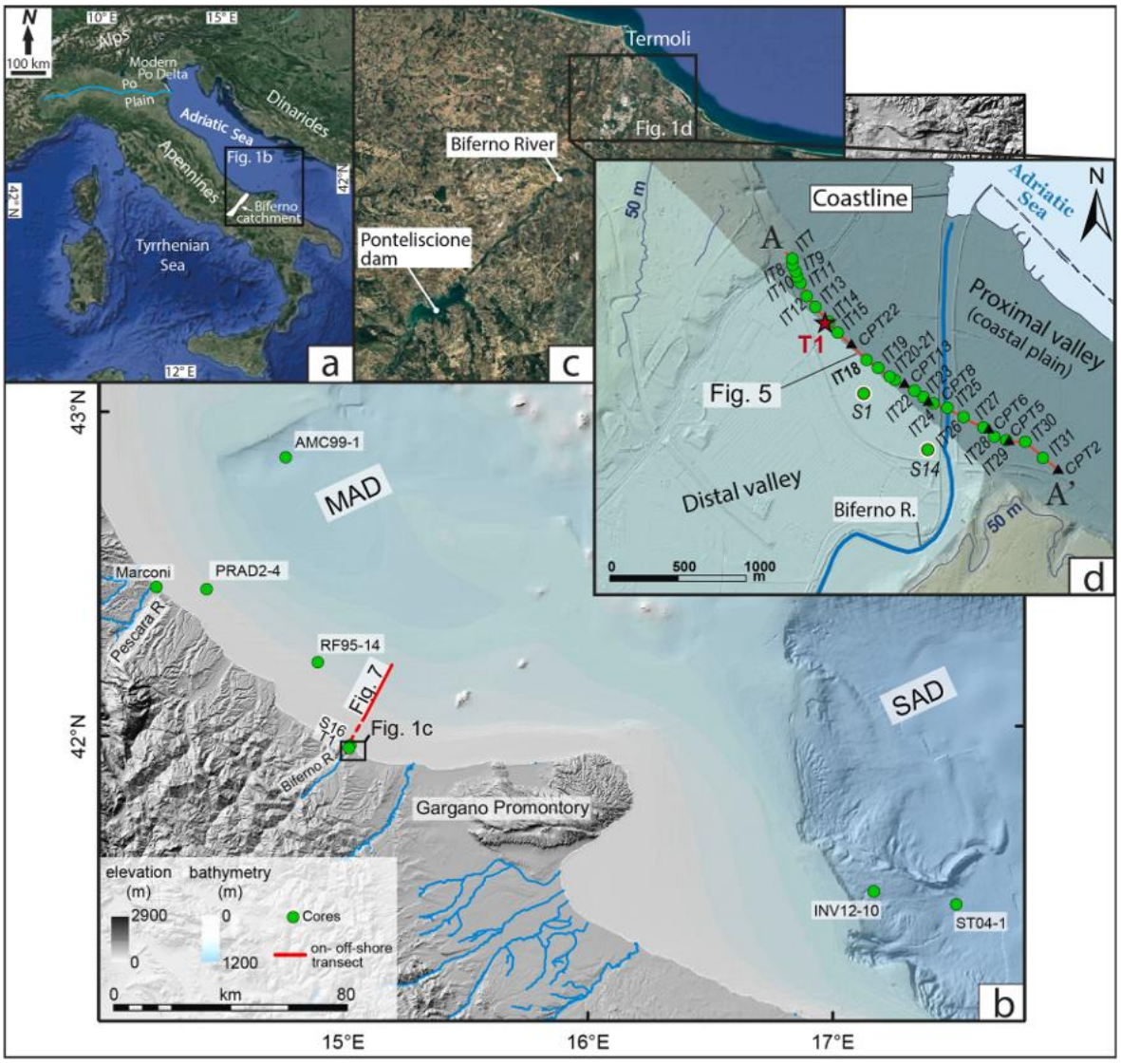

Fig. 1. – Study area and dataset. a) Study area within the Adriatic basin. b) Location of the sediment cores used in this study, and the trace of the stratigraphic panel of Fig. 7 c) The lower reaches of the Biferno River showing the location of the Ponteliscione dam. d) The Biferno coastal plain and the onshore dataset, including reference core T1, cone penetration tests (CPTs; black triangles) and continuous cores from Italferr S.p.A. (green circles). The locations of cores S1 and S14 (Amorosi et al., 2016a) are also shown. The red line indicates the trace of the stratigraphic panel shown by Fig. 5. (For interpretation of the references to color in this figure legend, the reader is referred to the Web version of this article.)

river incises a Quaternary foredeep succession composed of the Early Pleistocene Montesecco Clays, Early-Middle Pleistocene Serracapriola Sands, and Middle Pleistocene Campomarino Conglomerates (Amorosi et al., 2009; Bracone et al., 2011).

Beneath the modern Biferno coastal plain, in the study area (Fig. 1d), a multiple paleovalley system up to ~2 km wide and more than 50 m deep records repeated phases of incision and infilling since the Middle-Late Pleistocene (Fig. 2a). This paleovalley complex consists of superposed valleys incised into a Lower Pleistocene substrate (bedrock unit in Fig. 2a). According to Amorosi et al. (2016a), the earliest phases of valley formation have been related to long-term regional uplift, whereas the upper paleovalley system (Late Pleistocene-Holocene) developed mainly in response to glacio-eustatic sea-level fluctuations during the last glacial-interglacial cycle. Stepwise sea-level fall following Marine Isotope Stage (MIS) 5e promoted repeated episodes of fluvial incision, locally recorded by two buried fluvial terraces preserved along the southern valley flank and tentatively correlated with the MIS 5/4 and MIS 3/2 transitions, respectively (Amorosi et al., 2016a). The basal fill of the upper paleovalley comprises laterally amalgamated fluvial gravels, up to ~6 m thick, deposited during the Last Glacial Maximum (MIS 2), overlain by a mud-dominated succession up to 30 m thick consisting of alluvial silty clays, estuarine muds, and modern delta plain deposits (Fig. 2a).

2.2. The Adriatic Sea

The Adriatic Sea is a narrow epicontinental basin extending approximately 800 km along a NW-SE axis and conventionally subdivided into the Northern, Central and Southern Adriatic according to basin physiography (Bonaldo et al., 2016, Fig. 2b). The Northern Adriatic is characterized by a wide, gently dipping continental shelf extending to the Mid-Adriatic Depression (MAD; Fig. 2b), whereas the Southern Adriatic hosts the deepest sector of the basin (Southern Adriatic Depression, SAD; Fig. 2b), reaching water depths of ~1200 m (Cattaneo and Trincardi, 1999; Pellegrini et al., 2017, 2018; Trincardi et al., 1994). Since the Middle Pleistocene, repeated glacio-eustatic sea-level fluctuations have controlled accommodation and sediment dispersal, promoting basinward progradation during lowstands and

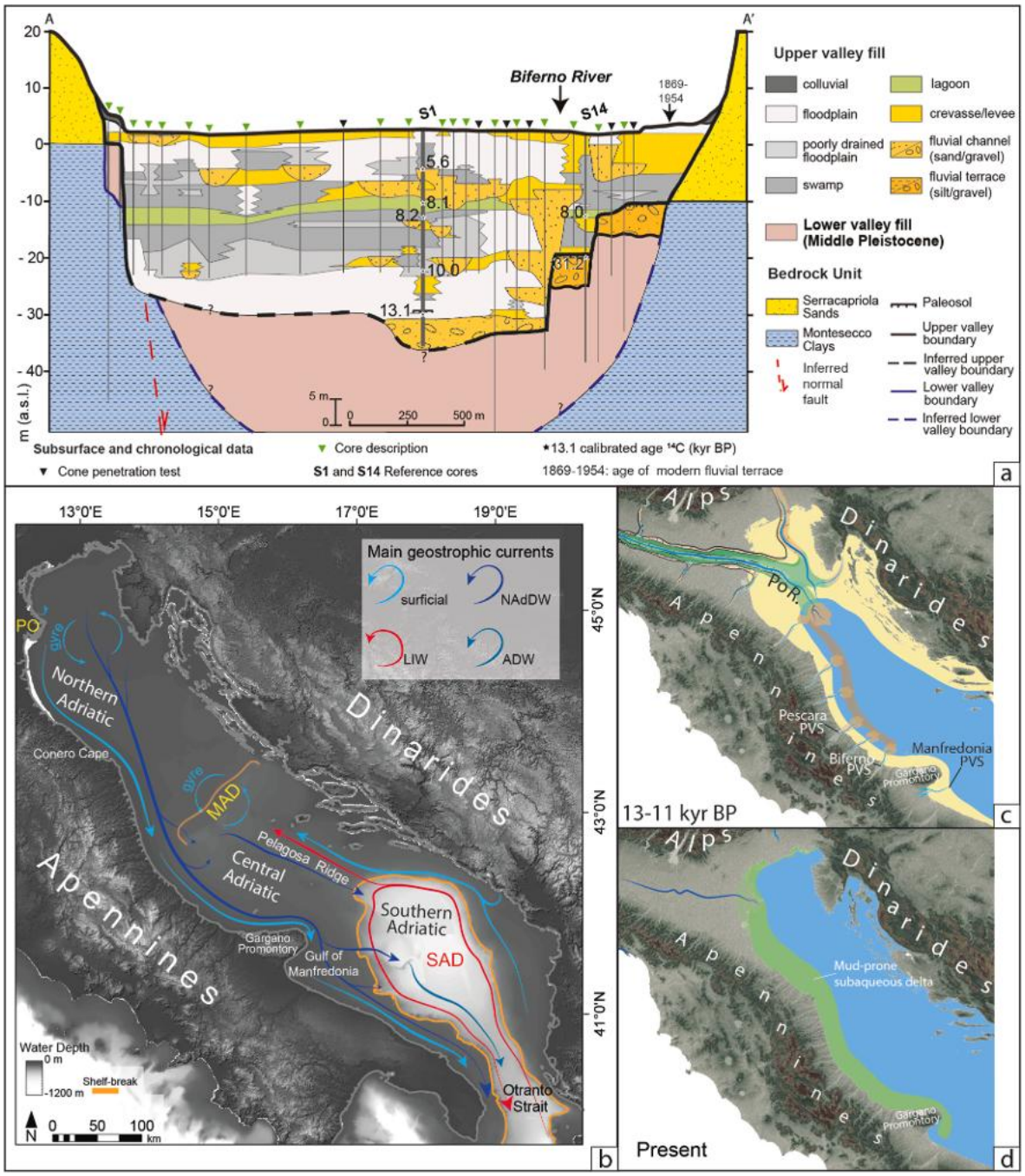

Fig. 2. – Stratigraphic and oceanographic background. a) Stratigraphic panel showing the stratal architecture of the Middle (lower) and Upper Pleistocene to Holocene (upper) Biferno paleovalley fill (modified from Amorosi et al., 2016a). b) Pathways of surface circulation in the Adriatic Sea. LIW: Levantine Intermediate Water. NAdDW: North Adriatic Dense Water. ADW: Adriatic Deep Water (modified from Amorosi et al., 2022). c) Paleogeography of the Adriatic basin at the Upper Pleistocene-Holocene (~13-11 cal kyr BP) with indication of paleovalley systems (PVSs). d) Present-day paleogeography of the Adriatic basin, with indication of the muddy subaqueous delta.

landward shoreline migration during transgressions (Dalla Valle et al., 2013; Zecchin et al., 2017).

Clastic sediment supply is dominated by rivers draining the Alps and the rapidly uplifting Apennines along the western margin (Amorosi et al., 2022; Cattaneo et al., 2003, Fig. 2b). Although the Po River drains the largest catchment, Apennine rivers contribute proportionally higher suspended sediment loads (Cattaneo et al., 2007). Under Holocene highstand conditions, the combined influence of fluvial input and cyclonic circulation promoted the formation of a laterally continuous, mud-dominated sedimentary wedge extending parallel to the Italian coastline (Cattaneo et al., 2003).

The basin-scale stratigraphic framework of the post MIS3/MIS2 succession has recently been documented by Campo et al. (2024). Above a regional erosional unconformity formed during the MIS3/2 sea-level fall, lowstand fluvial and deltaic deposits accumulated from the Last Glacial Maximum (LGM; MIS 2) until the onset of transgression (~14.4 cal kyr BP). They are overlain by transgressive deposits recording progressive shelf flooding (Correggiari et al., 1996; Pellegrini et al., 2015; Storms et al., 2008). The maximum flooding surface separates the backstepping transgressive succession from the overlying, prograding highstand muddy subaqueous delta extending along the western Adriatic margin from the modern Po River Delta down to the

Gargano Promontory (Fig. 2d; Cattaneo et al., 2003).

2.3. Oceanographic setting

The Adriatic Sea is characterized by a microtidal regime with predominantly cyclonic circulation driven by thermohaline forcing (Artegiani et al., 1997a; Poulain, 2001). A key component of this circulation is the Levantine Intermediate Water (LIW), which enters the Adriatic through the Otranto Strait (Fig. 2b) and contributes to the formation of North Adriatic Dense Shelf Water (NAdDW; Fig. 2b; Artegiani et al., 1997b; Orlić et al., 1994). Along the western Adriatic shelf, NAdDW flows southward approximately parallel to the Italian coastline, contributing to deep-water renewal while promoting the alongshore transport and redistribution of fine-grained sediments (Cattaneo et al., 2003, 2007; Chiggiato et al., 2016; Langone et al., 2016; Palinkas and Nittrouer, 2006; Pellegrini et al., 2021, 2024). Through cascading along the continental slope, NAdDW contributes to deep-water ventilation in the Southern Adriatic and, ultimately, in the Eastern Mediterranean (Bonaldo et al., 2016; Canals et al., 2009; Manca et al., 2002).

2.4. Sapropel S1 and organic matter in the western Adriatic basin

In deep-marine successions, intervals of basin-wide deoxygenation are recorded by organic carbon-rich layers known as sapropels (Rohling et al., 2015). In the Northern Hemisphere, sapropel formation has been primarily linked to enhanced freshwater input into the Eastern Mediterranean, largely conveyed by the Nile River system (Weldeab et al., 2014). Intensification of the African monsoon increased fluvial discharge and nutrient supply, promoting strong water-column stratification, a basin-wide weakening of thermohaline circulation, and enhanced primary productivity (De Lange et al., 2008). The most recent sapropel event, S1 (~10.2-6.8 cal ky BP), is associated with a major reorganization of Mediterranean circulation. At ~10.0 cal kyr BP (S1 onset), a weakening of the LIW circulation likely inhibited the formation of NAdDW, thereby diminishing deep-water ventilation in the Eastern Mediterranean and favoring widespread S1 deposition (Tesi et al., 2017). Critically low bottom-water oxygen concentrations were established at ~10.2 ± 0.3 cal kyr BP across large sectors of the basin (Schmiedl et al., 2010).

In the Southern Adriatic, OC content progressively increased from ~11 cal kyr BP, indicating a gradual deterioration of bottom-water oxygenation prior to S1 deposition (Rohling et al., 2015; Schmiedl et al., 2010). Similar trends have been documented elsewhere in the Eastern Mediterranean and are generally attributed to enhanced water-column stratification associated with increased freshwater input (Hennekam et al., 2014; Tachikawa et al., 2015). Such pre-freshening of the water column is widely regarded as a key prerequisite for sapropel formation (Grimm et al., 2015). A distinct interruption (S1 break), dated between ~8.3 and 7.8 cal kyr BP in the Adriatic, subdivides S1 into S1a (~10.2-8.3 cal kyr BP) and S1b (~7.8-6.8 cal kyr BP), and is commonly interpreted as a temporary phase of bottom-water reoxygenation (Marino et al., 2009; Tesi et al., 2017).

Organic Matter (OM) preserved in western Adriatic sediments derives from both terrigenous (allochthonous) and marine (autochthonous) sources (Tesi et al., 2007). Marine OM is mainly ascribed to marine and estuarine phytoplankton, zooplankton and fecal pellets (Boldrin et al., 2005; Miserocchi et al., 2007), whereas terrigenous inputs are represented by soil-derived OM, plant debris and riverine/lacustrine phytoplankton. These end-members display distinct elemental and isotopic signatures, allowing changes in OM provenance to be evaluated using bulk geochemical proxies such as TOC, TN, $\delta^{13}C$, and $\delta^{15}N$ (Fry and Sherr, 1984; Sánchez Goñi et al., 2005; Tesi et al., 2007). Along the western Adriatic sector, suspended material is dominated by marine and estuarine phytoplankton, whereas riverine and coastal sediments are largely enriched in terrestrial organic matter. In the modern Biferno coastal plain, soil-derived OM represents the dominant component of surficial sediments, and part of this fine-grained terrestrial material is transported southward along the western Adriatic shelf by the prevailing circulation (Pellegrini et al., 2021; Tesi et al., 2007).

3. Material and methods

This work revisits the subsurface stratigraphic interpretation of the Biferno paleovalley system proposed by Amorosi et al. (2016a; Fig. 2a) by integrating new sedimentological, paleoecological, geochemical, and chronological analyses from the newly recovered continuous sediment core T1. Following the stratigraphic reconstruction of Amorosi et al. (2016a), reference core T1 (42.6 m long) was recovered from the depocentral sector of the Biferno paleovalley (41°58′13.4"N, 15°01′00.1"E; Fig. 1d), where the Upper Pleistocene-Holocene succession reaches its maximum thickness and the S1-equivalent interval is likey best preserved. The core was specifically acquired to recover a complete S1-equivalent succession for detailed multiproxy characterization. In addition, the subsurface dataset provided by Italferr S.p.A. (Ferrovie dello Stato Italiane Group) includes 25 boreholes with depths ranging from 20 to 60 m and 6 cone penetration tests (CPTs) reaching depths of 15-30 m.

3.1. Facies analysis, stratigraphic correlation and volume estimates

Detailed facies interpretation was based on the integration of sedimentological and paleontological (benthic foraminifer and ostracod) investigations performed on core T1. Texture, mean grain-size, color, sedimentary structures, and accessory components, such as mollusk content, plant remains, wood fragments, and carbonate concretions were described (Fig. 3). Compressive strength (pocket penetrometer) measurements, which are particularly diagnostic of fine-grained deposits (silts and clays), were also considered following the criteria outlined by Amorosi et al. (2015).

Core data (facies boundaries) were used to calibrate CPT profiles, with particular emphasis on tip resistance (qc) and sleeve friction (fs) values, as shown by Campo et al. (2023). Tip resistance reflects the force required to advance the cone through the sediment, whereas sleeve friction records the resistance acting on the cone sleeve. In this study, qc values were primarily used to facilitate the identification of coarse-grained sedimentary bodies in the subsurface, whereas integrated qc and fs allowed distinction between poorly-consolidated (PVF) vs more consolidated (paleosols or substrate) strata. The subsurface stratigraphy of the Biferno coastal plain was reconstructed along a shore-parallel, NW-SE transect crossing the Biferno valley approximately 1.5 km landward of the modern coastline (Fig. 1d).

For meiofauna analysis, 58 samples (Table 1) of ca. 100 g were collected along core T1 to refine facies characterization. Sediment samples were prepared at Bologna University laboratories, following a standard procedure (e.g. Rossi and Vaiani, 2008): (i) dried for 8 h at 60°C, (ii) soaked in water, (iii) wet sieved through sieves of 63 μm, (iv) dried again for at least 8 h and weighted, and (v) dry sieved at 125 μm. Size fractions >125 μm and 63-125 μm were analyzed separately. Species identification was based upon original descriptions (Ellis and Messina, 1940, 1952) and reference papers that were also used for paleoenvironmental interpretations (Athersuch et al., 1989; Bonaduce et al., 1975; Cimerman and Langer, 1991; Hayward et al., 2025; Henderson, 1990; Jorissen, 1988), integrated by other selected papers (Barbieri and Vaiani, 2018; Murray, 2006; Rossi et al., 2024; Salel et al., 2016)

First-order sediment volumes for the $S1a_{eq}$, $S1break_{eq}$, and $S1b_{eq}$ intervals were estimated from the reconstructed areal (planform) dimensions and representative thicknesses of the corresponding paleovalley depocenters, based on the well-constrained Biferno and Pescara paleovalley systems. For each interval, volume was approximated as the

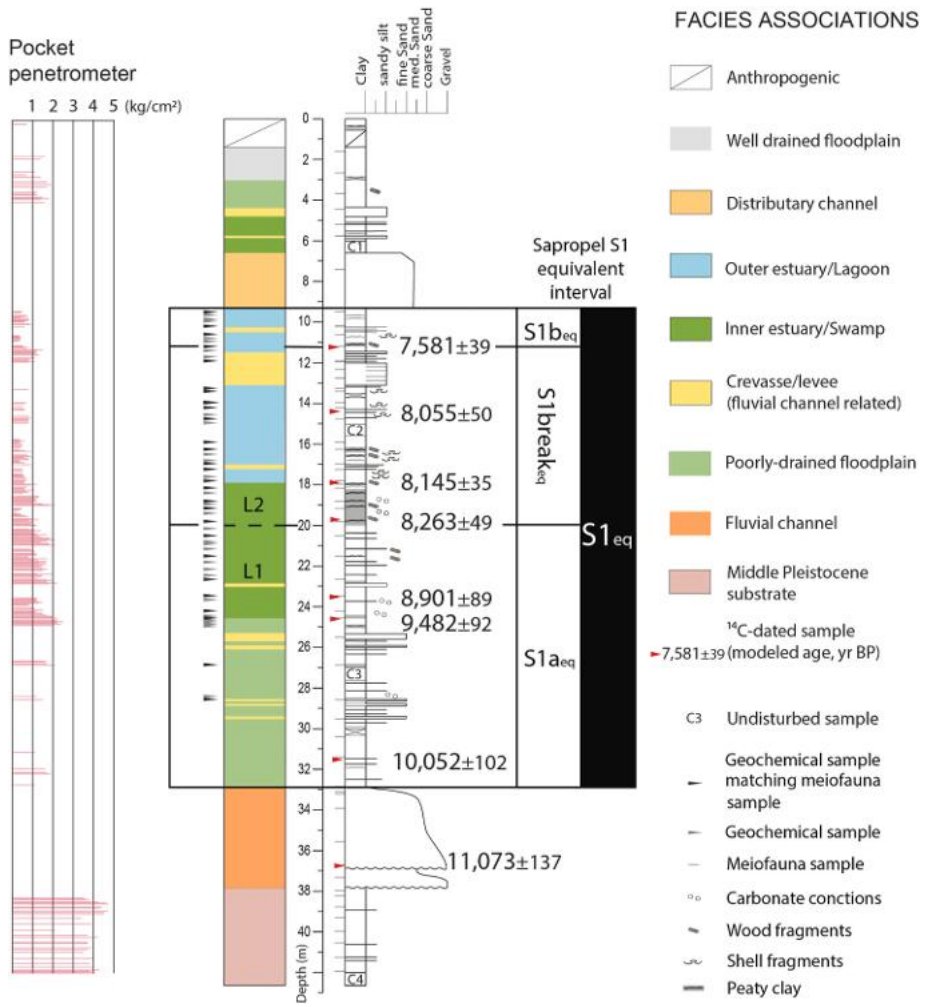

Fig. 3. – Stratigraphic log of the reference core. Facies interpretation and pocket penetrometer measurements of core T1 (see Fig. 1 for location). Modeled radiocarbon ages (cal yr BP) are shown on the right. The investigated succession represents the terrestrial equivalent of the sapropel S1 event. S1a$_{eq}$: S1a-equivalent interval; S1break$_{eq}$: S1 break-equivalent interval; S1b$_{eq}$: S1b-equivalent interval.

product of its estimated length, width and mean thickness, assuming a simplified prism geometry. These dimensions represent first-order approximations of the portions of the paleovalley systems occupied by the corresponding S1eq depocenters and do not account for detailed three-dimensional geometries, lateral facies changes, or the progressive landward migration of the systems during transgression.

3.2. Chronology

The chronostratigraphic framework is primarily based on eight ^{14}C ages obtained from organic-rich samples retrieved from the T1 borehole. These new ages are complemented by three previously published ^{14}C ages from core S1 and two from core S14 (Amorosi et al., 2016a), which provide additional chronological constraints for the stratigraphic correlation across the Biferno paleovalley fill.

Radiocarbon measurements were performed at the KIGAM Laboratory (Daejeon, Republic of Korea) following standard acid-alkali-acid pretreatment. Prior to analysis, all new samples were washed with deionized water and dried at 40°C to inhibit fungal growth. The resulting ^{14}C ages were initially calibrated against the IntCal20 atmospheric calibration curve using OxCal 4.4 (Ramsey, 1995; Ramsey and Lee, 2013).

The eight new ^{14}C ages from core T1 were subsequently used to construct a Bayesian age-depth model employing the P_Sequence depositional model within OxCal (see Supplementary material), which assumes a Poisson distribution for depositional events (Ramsey, 2008, 2009). By incorporating stratigraphic depth as prior information, this modeling approach allows for the identification of potential outliers and facilitates minor adjustments to individual age estimates within the sequence. Hereafter, the term “modeled age" refers to the posterior age estimate produced by the Bayesian age-depth model, which integrates the calibrated ^{14}C ages with the stratigraphic constraints imposed by the depositional model. Accordingly, all stratigraphic interpretations are based on modeled ages rather than on independently calibrated ^{14}C dates.

Furthermore, the age-depth model enables a reliable estimation of sedimentation rates throughout the succession. The final age-depth plot illustrates the modeled probability density functions, with uncertainty ranges consistently reported at the 95.4% confidence interval. Unless otherwise specified, all ages discussed hereafter refer to modeled ages derived from the Bayesian age-depth model.

3.3. Elemental and stable isotopic analyses

The stable isotope composition of organic carbon and nitrogen (δ^{13}C and δ^{15}N), together with bulk total organic carbon (TOC) and total nitrogen (TN) contents, were determined for 56 samples from core T1 (Table 1). Sampling intervals were defined based on the existing chronostratigraphic framework (Amorosi et al., 2016a; Tesi et al., 2017) and the sampling strategy was designed to ensure representative coverage of

Table 1
– Depths (m) of T1 core samples selected for meiofauna (n = 58) and geochemical (n = 56) analyses.

Meiofauna analysis		Geochemical analysis	
Sample depth (m)		Sample depth (m)	
1.6	19.15	9.5	18.8
2.65	19.8	9.65	18.95
3.7	20.5	9.85	19.15
4.45	21.5	9.95	19.4
5.2	22.65	10.2	19.8
5.75	23.45	10.6	20.15
7.4	24.2	10.8	20.5
9.5	24.55	10.95	20.8
10.2	25.5	11.2	20.9
10.2 bis	26.85	11.4	21.15
10.6	28.55	11.7	21.5
11.2	29.52	11.9	21.8
11.9	30.38	13.25	22.15
11.95	31.38	13.4	22.45
12.3	32.83	13.95	22.65
12.75	33.08	14.2	23.45
13.25	33.2	14.55	23.65
13.4	33.9	14.75	24.2
13.95	35.54	14.95	24.45
14.2	36.7	15.9	24.55
14.75	37.3	16.25	24.65
15.9	37.95	16.5	24.75
16.25	38.2	16.8	24.85
16.95	38.75	16.95	24.95
17.25	39.28	17.23	26.85
17.8	39.95	17.6	28.4
17.95	40.52	17.8	28.55
18.15	41.25	18.15	
18.8	41.93	18.4	

the main facies associations of the S1 equivalent succession.

Approximately 15 mg of freeze-dried and homogenized sediment were weighed into silver capsules and treated with 1.5 M HCl to remove inorganic carbon. After acidification, the material was dried at 55°C prior to elemental and isotopic measurements. Analyses were carried out using a Thermo Scientific FLASH 2000 CHNS elemental analyzer coupled to a Thermo Delta V (Delta Q) isotope ratio mass spectrometer (IRMS) via a CONFLO IV interface at the Institute of Polar Sciences, National Research Council (CNR-ISP).

Isotope ratios are expressed in δ notation as per mil (‰) relative to international standards, Vienna Pee Dee Belemnite (VPDB) for carbon and atmospheric N_2 (AIR) for nitrogen. Analytical precision, evaluated through repeated measurements of in-house standards, was better than ±0.15‰ for $\delta^{13}C$ and ±0.25‰ for $\delta^{15}N$, the latter calibrated against an ammonium sulfate standard. The relative standard deviation (RSD) for bulk TOC and TN contents was below 5%, based on replicate analyses of laboratory reference materials.

4. Results

4.1. Facies associations

Facies analysis led to the identification of 8 facies associations above the Middle Pleistocene substrate (Fig. 3). Substrate characteristics and facies associations are described below in stratigraphic order. The identification of the terrestrial equivalent of Sapropel S1 ($S1_{eq}$), including $S1a_{eq}$ (~10.0-8.3 cal kyr BP), S1 $break_{eq}$ (~8.3-7.6 cal kyr BP), and $S1b_{eq}$ (~7.6-6.8 cal kyr BP) intervals (Fig. 3), was based on the modeled ages derived from the Bayesian age-depth model (see Table 2).

4.1.1. Middle Pleistocene substrate

Description. This unit is composed of grey to brownish clay and silty clay, locally interbedded with centimeter-thick sand layers (Fig. 4). Horizontal lamination is common, while bioturbation is sporadically observed. This unit was encountered at the base of core T1, below ~42.0 m depth (Figs. 3 and 5). It displays consistently high pocket penetration (Pp) values, exceeding 4 kg/cm^2 (Fig. 3). Sleeve friction fs is generally higher than 1.0 kg/cm^2. Foraminiferal assemblages include few, poorly preserved specimens. Planktonic foraminifera (mainly *Globigerina*) are more abundant than benthic forms, which are represented by *Ammonia beccarii*, *Cassidulina laevigata*, and *Gyroidina umbonata*. Ostracods are extremely rare and include valves of genera *Xestoleberis* and *Hiltermannicythere*.

Interpretation. Sedimentological features, lithology and the clearly reworked meiofauna, including marine taxa thriving at incompatible water depths, reflect deposition in a low-energy continental depositional environment. This interpretation is consistent with previous stratigraphic reconstructions (Amorosi et al., 2016a), which recognized a thick floodplain succession within the lower-PVF.

4.1.2. Fluvial-channel facies association

Description. This facies association (~38-33 m depth in core T1, Fig. 3), with a maximum thickness of ~5 m, is dominated by amalgamated, poorly-sorted gravel deposits including rounded calcareous pebbles and cobbles, and gravelly sand locally supported by a silty-sand matrix (2-10 cm in diameter; Fig. 4). This facies association is bounded at the base by a sharp erosional surface incising the underlying substrate and consists of two vertically-stacked gravel bodies showing distinct fining-upward trends (Figs. 3 and 4). Microfossils are absent, and no

Table 2
– Radiocarbon ages used in this study for the T1 core. The table reports conventional ^{14}C ages, calibrated ages with their 95.4% confidence intervals (*2σ*), and modeled ages with their associated uncertainties derived from the OxCal Bayesian age-depth model.

Sample Code	Material	Core Name and Depth	^{14}C age (BP)	Error (yr)	Calibrated age (2σ range, cal BP)		Calibrated age (cal BP)	Error (yr)	Modeled age (cal BP)	Error (yr)
KGM-OWd250070a	organic clay	T1_11.25	*6711*	*32*	*7662*	*7510*	*7579*	*38*	*7581*	*39*
KGM-OWd250071a	organic clay	T1_14.40	*7290*	*33*	*8174*	*8023*	*8104*	*46*	*8055*	*50*
KGM-OWd250072a	organic clay	T1_17.90	*7304*	*30*	*8176*	*8029*	*8105*	*44*	*8145*	*35*
KGM-OWd250073a	organic clay	T1_19.75	*7451*	*36*	*8355*	*8185*	*8267*	*50*	*8263*	*49*
KGM-OWd250074-1	organic clay	T1_23.55	*8016*	*35*	*9012*	*8724*	*8879*	*81*	*8901*	*89*
KGM-OWd250075a	organic clay	T1_24.60	*8461*	*38*	*9535*	*9430*	*9489*	*34*	*9482*	*92*
KGM-OWd250076-1	organic clay	T1_31.65	*8871*	*41*	*10178*	*9775*	*10006*	*128*	*10052*	*102*
KGM-OWd260035	Wood fragment	T1_36.75	*9688*	*53*	*11229*	*10793*	*11107*	*128*	*11073*	*137*

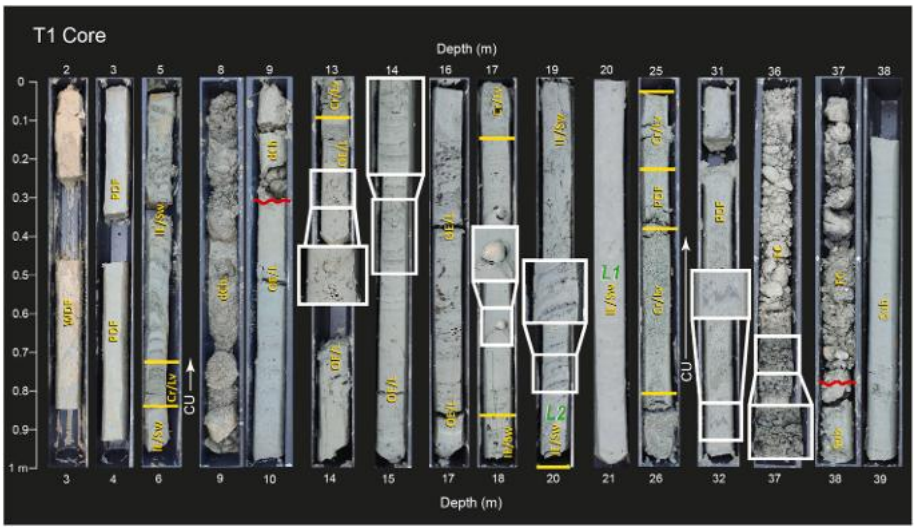

Fig. 4. – Representative photographs of the substrate and facies associations in core T1. Middle Pleistocene alluvial substrate (Sub). Fluvial-channel (FC) gravels with erosional basal boundary (red-wavy line) and detail of a coarse sand interval. Massive grey silts and clays of poorly-drained floodplain (PDF) facies association, with close-up showing thin layers of decomposed organic matter and charcoal fragments. Crevasse/levee (Cr/Lv) sandy silt to silty sand, showing an overall coarsening-upward (CU) trend. Typical inner estuary/swamp (IE/Sw; *L1*: lithofacies 1; *L2*: lithofacies 2) and outer estuary/lagoon (OE/L) deposits, with details on decomposed organic matter/wood fragments within IE/Sw and *Cerastoderma glaucum*/shell fragments within OE/L. Distributary channel (dCh) sands with erosional lower base cutting into older IE/Sw facies. Mottled well-drained floodplain (WDF) clay and silty clay. (For interpretation of the references to color in this figure legend, the reader is referred to the Web version of this article.)

mollusk shells were observed. A wood fragment was encountered at 36.75 m depth yielded an age of ~11.1 cal kyr BP (Table 2; Fig. 3). Gravel bodies were not penetrated by piezocone penetration tests, except for their uppermost, finer-grained intervals, which yielded tip resistance (qc) values lower than 200 kg/cm^2.

Interpretation. The very coarse grain size, internal fining-upward organization, and erosional lower boundary indicate deposition within a high-energy fluvial-channel depositional environment (Miall, 2013). Poor sorting, clast-supported textures, and amalgamation surfaces point to a braided river style developed under conditions of high discharge and steep longitudinal gradients. These deposits are interpreted as fluvial channel fills formed within the narrow piedmont sector of the Biferno Valley (Fig. 1d). The lack of fossils is consistent with this interpretation.

4.1.3. Channel-related facies association

Description. This facies association was encountered at various depths in core T1 (~29.5-28.5 m, ~26-25.5 m, ~23 m, ~17 m, ~13-11.5, ~10.5 m, ~6-4.5 m; Fig. 3) and comprises three main lithofacies. The first includes silty sand deposits, up to ~1.0 m thick, characterized by fining-upward trends, erosional basal contacts, and gradational upper boundaries (Fig. 4). The second lithofacies consists of sandy silt to silty sand bodies, a few decimeters thick, showing an overall coarsening-upward tendency, with gradational lower boundaries and sharp tops. The third lithofacies is represented by rhythmic millimeter-to centimeter-scale alternations of grey to brownish silty sand, silt, and clayey silt (Fig. 4). Silty intercalations are locally present, together with sparse wood fragments. Fe-, Mn-, and $CaCO_3$ nodules, as well as plant debris, occur locally. These heterogeneous deposits are encountered throughout the Holocene succession (Fig. 3). Samples are barren of fossils or contain rare and poorly preserved foraminifera. Tip resistance values range between 40 and 80 kg/cm^2 in the silty sand-clay alternations and between ~90 and 120 kg/cm^2 in the silty sand bodies.

Interpretation. Sedimentological features and the absence of an autochthonous meiofauna indicate deposition in a range of fluvially dominated sub-environments located close to the river axis. The occurrence of plant remains suggests overbank settings repeatedly affected by flooding. Thin sand bodies displaying coarsening-upward trends and gradational bases are interpreted as crevasse splay deposits (CrS), whereas fining-upward sandy units with erosional basal contacts are attributed to crevasse channel fills (CrC). The rhythmic alternation of silty sand and silt is interpreted as proximal overbank (levee) deposits (Lv), reflecting tractional transport combined with suspension fallout.

4.1.4. Poorly-drained floodplain facies association

Description. This facies association consists of individual bodies generally less than ~1.5 m thick, occurring predominantly between ~33 and 24.5 m depth in core T1 (Figs. 3 and 4), and is composed of massive grey to dark-grey clays and silty clays (Fig. 4). Silty sand interbeds, ranging from a few millimeters to centimeters in thickness, are locally present (Figs. 3 and 4). Thin layers of decomposed organic matter, a few centimeters thick, are commonly encountered (31.9, 29.9, 28.5 m depth; Fig. 4), whereas dispersed wood and charcoal fragments as well as carbonate nodules may locally occur (Fig. 4). Oxidation features, such as Fe-Mn oxides, are absent. This facies association occurs in core T1 between ~33 and 24.55 m and ~4.4-3 core depths (Fig. 3). The lowermost interval is barren of meiofauna, while few scattered valves of *Ilyocypris* spp. and *Cyprideis torosa* are recorded around 4 m core depth. Scattered fragments of continental gastropods are present. Pocket penetrometer values range from 1.0 to 2.2 kg/cm^2 (Fig. 3), while cone tip resistance values are low, generally between ~10 and 22 kg/cm^2. Radiocarbon ages constrain deposition of this facies association mostly between ~10.2 and 9.5 cal kyr BP (Fig. 3 and Table 2).

Interpretation. The dominance of fine-grained sediments, presence of vegetal remains/organic-rich layers and sporadic hypohaline-euryhaline ostracods, and geotechnical characteristics are consistent with a depositional environment characterized by low relief, frequent overbank flooding and commonly high-water tables, typical of poorly drained floodplain conditions. The occurrence of carbonate nodules, associated with frequent water table variations, and the absence of Fe-Mn oxides indicate deposition in a low-energy setting not subject to long-lasting phases of subaerial exposure, and are consistent with this interpretation. All these characteristics are typical of a transitional setting between well-drained floodplain and paludal environments.

4.1.5. Inner estuary/swamp facies association

Description. This facies association attains a maximum thickness of ~6.5 m in core T1, between 24.5 and 18 m depth (Fig. 3), and consists of two main lithofacies. Lithofacies 1 (L1) is characterized by massive clay and silty clay ranging in color from grey to darkish grey where decomposed organic matter occurs (Fig. 4). Scattered and millimeter-scale wood fragments can be locally encountered (Fig. 4). Lithofacies 2 (L2) is composed of very soft dark-grey to blackish clays, rich in organic matter, with abundant millimeter-to centimeter-scale plant debris and wood fragments (Fig. 4). Thin peat layers (generally a few centimeters thick) occur at several stratigraphic levels, preferentially within lithofacies 2. Silt and silty sand interbeds, a few centimeters thick, are locally present. Within L1 ostracods are common and mainly represented by *Cyprideis torosa*, with rare valves of *Loxoconcha stellifera*, *Xestoleberis dispar,* and *Heterocypris salina*. Few benthic foraminifera (*Ammonia tepida* and *Ammonia parkinsoniana*) are observed. Within L2 the meiofauna is almost absent or extremely scarce (a few valves of *C. torosa*). Pocket penetrometer and CPT tip resistance values are consistently low for L2 (<1 kg/cm^2 and <10 kg/cm^2, respectively), with slightly higher values (up to ~1.8 kg/cm^2 and ~18 kg/cm^2) recorded within peaty intervals and L1 (Fig. 3). This facies association dominates the stratigraphic interval between ~24.55 and 18 m and ~6.5-4.8 m core depth, overlying and underlying poorly-drained floodplain deposits, respectively (Fig. 3). Between ~24.55 and 18 m depth, L1 is overlain by L2. Radiocarbon ages constrain deposition of this facies mainly between ~9.5 and 8.2 cal kyr BP (Fig. 3; Table 2).

Interpretation. The fine-grained lithology, high to extremely high organic content, presence of peat horizons and very low penetration resistance values indicate deposition in a low-energy, permanently waterlogged setting with a vegetated bottom. The absence of oxidation features, scarcity of sand and dominance of organic-rich sediments are consistent with reducing conditions typical of paludal environments away from active fluvial channels (Bruno et al., 2019). The occurrence of a meiofauna dominated by euryhaline species suggests incursions of slightly saline waters, while sterile horizons likely reflect poorly oxygenated conditions. Overall, the assemblage and sedimentological characteristics point to weakly brackish conditions, typical of marsh or salt-marsh environments developed in the inner estuarine sector or on the upper delta plain (Amorosi et al., 2017; Rossi et al., 2024).

4.1.6. Outer estuary/lagoon facies association

Description. This facies association attains a maximum thickness of ~4 m in the reference core between ~18 and 9.5 m depth (Fig. 3) and is composed predominantly of very soft grey clays. Faint lamination and millimeter-thick sandy-silt interbeds are locally observed, particularly between 14.30 and 14.60 m core depth (Fig. 4). Wood fragments and vegetal remains occur throughout the unit, but preferentially in the lower interval, between 16.15 and 16.8 m depth (Fig. 4). *Cerastoderma glaucum* was identified in the lower interval between 17.8 and 17.15 m depth (Fig. 4). Upward, this facies association is intercalated with crevasse silty sands (between ~14 and 13 m core depth) and is overlain by distributary channel sands (Figs. 3 and 4). Microfossils are abundant and well preserved, with relatively diversified assemblages; the maximum amount of miliolids was observed at 14.75 m core depth. In general, the foraminiferal assemblage includes *Haynesina germanica*, *Ammonia tepida, A. parkinsoniana*, with subordinate *Porosononion granosum*, *Cribroelphidium* spp. and miliolids (e.g., *Massilina secans, Miliolinella subrotunda* and *Quinqueloculina* spp.). Ostracods are more common than benthic foraminifera and show the dominance of *Cyprideis torosa*, accompanied by *Loxoconcha* (*L. elliptica*, *L. stellifera*), *Xestoleberis* (*X. dispar*, *X. decipiens*), and *Leptocythere* (*L. bacescoi*, *L. ramosa*) species between ~15 and 13 m core depth. These subordinate taxa are particularly well-represented within the ostracod assemblage at 14.75 m core depth. CPT tip resistance and pocket penetrometer values range between ~5 and 11 kg/cm^2 and ~0.4-1 kg/cm^2 (Fig. 3), respectively. Radiocarbon ages constrain deposition of this unit between ~8.2 and > 7.7 cal kyr BP (Fig. 3).

Interpretation. The clay lithology, low sediment consistency and dominance of euryhaline species (*Haynesina germanica*, *Ammonia tepida, A. parkinsoniana*, *C. torosa*) indicate deposition in a low-energy, brackish environment consistent with a lagoon or outer estuary (Rossi et al., 2024). Ostracods and foraminifers suggest the most pronounced marine influence at 14.75 m depth, where the highest species diversity and the highest amount of typical marine taxa (miliolids, *L. ramosa*) were observed.

4.1.7. Distributary channel facies association

Description. This facies association occurs in the uppermost ~10 m of core T1 between ~9 and 6.5 m depth, interbedded within outer and inner estuary deposits (Fig. 3). It is mainly composed of sand bodies up to ~3 m thick, with an erosional basal surface (Fig. 4) and a well-developed fining-upward trend, from coarse-to medium-grained grey sands at the base to silty sands (Fig. 3). Centimeter-thick silt-clay intercalations and scattered pebbles are locally preserved. The meiofauna is generally absent. CPT data show high tip resistance values (qc up to ~200 kg/cm^2), with a systematic decrease upward, consistent with progressive fining.

Interpretation. The erosional lower boundary, lithology and fining-upward tendency support interpretation as fluvial-channel deposits formed under high-energy, non-marine conditions (Bridge, 2006). The absence of microfossils further corroborates this interpretation. The upward and lateral transition to paludal clays, together with decreasing grain size, suggests deposition within distributary channels in a low-energy upper delta-plain environment (Bhattacharya, 2006).

4.1.8. Well-drained facies association

Description. This facies association occurs in the uppermost ~3 m of core T1 (Figs. 3 and 4). The facies is composed of rooted, pedogenized grey to brownish clays and silty clays, commonly mottled by Mn-Fe oxides. Silty sand intercalations and carbonate nodules are locally present. Well-developed paleosols were identified in cores S1 and S14 (Fig. 2a; Amorosi et al., 2016a), displaying dark, organic-rich A horizons overlying grey clay with oxide mottling and carbonate nodules (Bk horizons). The meiofauna is absent, while shell-rich horizons may locally contain continental mollusks. This facies association is in lateral transition to pedogenized levee/crevasse deposits and poorly drained floodplain clays. CPT data show moderate tip resistance values (qc = 15-25 kg/cm^2), while pocket penetration values range between 1.5 and 1.8 kg/cm^2, locally reaching ~3 kg/cm^2 within paleosols.

Interpretation. This facies association represents the deposits of the modern coastal plain. Lithological attributes, pedogenic features and geotechnical properties indicate deposition in a well-drained floodplain. Fine-grained sediments, root traces and pedogenized horizons reflect low-energy accumulation under subaerial exposure and a persistently low water table. The occurrence of continental mollusks further supports this interpretation. Paleosols characterized by A-Bk horizons are interpreted as Inceptisols (Soil Survey Staff, 1999) and likely record phases of non-deposition and landscape stability lasting several thousand years. Penetration resistance values are consistent with well-drained floodplain deposits, in agreement with previous studies from comparable alluvial-coastal settings (Amorosi et al., 2014; Amorosi and Marchi, 1999; Sarti et al., 2012).

4.1.9. Anthropogenic facies association

Description. This facies association, about 1.5 m thick, occurs at the top of the stratigraphic succession in the reference core (Fig. 3). It consists of chaotic, unconsolidated and poorly sorted deposits composed of materials of mixed provenance. Natural components (sediment, wood fragments) coexist with anthropogenic materials, including bricks, plastic and metal fragments. Clasts range from blocks to cobbles, display angular to rounded shapes, and lack any systematic fabric or internal organization. Sedimentary structures are absent.

Interpretation. The stratigraphic position at the top of the succession, the absence of depositional structures, and the presence of anthropogenic materials indicate an origin related to human activity. The poorly-sorted, unconsolidated nature of the deposits is consistent with landfill or backfill operations, whereas intervals dominated by sub-angular clasts are interpreted as remnants of construction-related foundations.

4.2. Stratigraphic architecture and paleoenvironmental evolution

The sedimentological analysis of core T1 and stratigraphic correlation with adjacent boreholes allowed the construction of the stratigraphic panel shown in Fig. 5. The panel builds upon the stratigraphic framework proposed by Amorosi et al. (2016a) and documents the architecture of multiple phases of valley incision and infilling over the last ~400 kyr. Below the erosional unconformity marking the base of the Upper Pleistocene-Holocene paleovalley system (PVS), the overconsolidated fine-grained deposits recovered in the lower part of core T1 have previously been interpreted as the infill of older (Middle Pleistocene) paleovalley systems and are herein referred to as Middle Pleistocene substrate. Likewise, isolated gravel bodies unconformably overlying the Middle Pleistocene substrate at shallow depths have previously been interpreted as fluvial terrace deposits formed during the long phase of sea-level fall between MIS 5e and MIS 2 and assigned to the falling stage systems tract (FSST; Fig. 5).

Amalgamated gravels with a cumulative thickness of approximately 5 m form a laterally continuous fluvial body between 31 and 36 m b.s.l. (Fig. 5). These deposits correlate with the basal gravel body previously identified in core S1 and record fluvial sedimentation from the LGM (MIS 2) through the final stages of the Younger Dryas and into the earliest phase of post-Younger Dryas sea-level rise, as indicated by the new ~11.2 cal kyr BP age (Fig. 5). The newly acquired T1 core allowed this fluvial body to be traced continuously across the PV depocenter for approximately 1 km (Fig. 5). Its geometry and lithological characteristics indicate deposition within a laterally extensive, high-energy braided fluvial system confined within a narrow (~1 km wide) valley. The absence of associated finer-grained alluvial deposits further supports this interpretation. Accordingly, the erosional surface at the base of the amalgamated fluvial gravels was interpreted as the sequence boundary separating the Upper Pleistocene-Holocene PVF from the underlying Middle Pleistocene succession (Fig. 5).

The upward transition to well-drained deposits in core S1, between 32 and 30 m b.s.l. (Fig. 5), is accompanied by a decrease in the degree of fluvial channel amalgamation, indicating a transition from braided to meandering fluvial systems. In paleovalley successions, this change has previously been interpreted as the inland expression of the transgressive surface (Tanabe et al., 2006). Chronological data constrain this mud-dominated continental interval to between 14.4 and 13.1 cal kyr BP. A pedogenized horizon dated to 13.1 cal kyr BP is tentatively correlated with the YD interval (12.9-11.7 cal kyr BP, Broecker et al., 2010). Above this horizon, the succession displays a progressive deepening-upward trend from continental to increasingly marine-influenced deposits, culminating in the establishment of

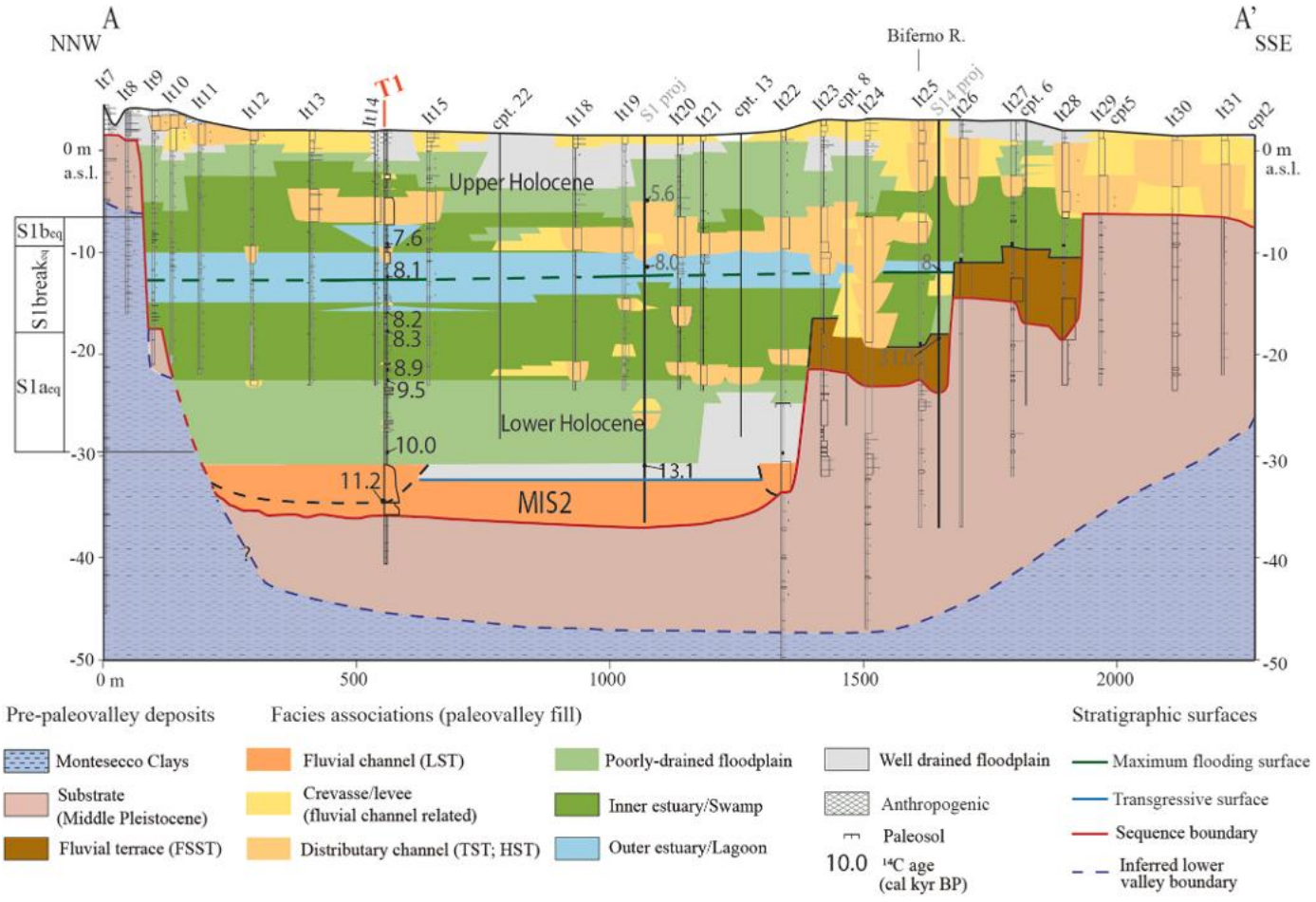

Fig. 5. Stratal architecture of the Biferno paleovalley fill. Stratigraphic panel illustrating the transverse facies architecture of the Upper Pleistocene-Holocene paleovalley fill beneath the modern Biferno coastal plain (location in Fig. 1d). The panel also highlights the intervals corresponding to the onshore counterparts of Adriatic S1a (~10.0-8.3 cal kyr BP), S1 break (8.3-7.6 cal kyr BP), and S1b (~7.6-6.8 cal kyr BP). FSST: Falling stage systems tract; LST: Lowstand systems tract; TST: Transgressive systems tract; HST: Highstand systems tract.

estuarine conditions (Fig. 5).

A ^{14}C age of ~10.0 cal kyr BP above the YD fluvial deposits constrains the overlying mud-dominated PVF, characterized by isolated fluvial sand bodies, to the Holocene (Fig. 5). The Lower Holocene succession (~10.0-8.1 cal kyr BP) encompasses the sapropel S1a-equivalent ($S1a_{eq}$) and a large portion of the S1 break-equivalent interval ($S1break_{eq}$), reaching a maximum thickness of approximately 19 m (31-12 m b.s.l.; Fig. 5). The $S1a_{eq}$ (~10.0-8.3 cal kyr BP) consists of a vertical succession of continental to organic-rich estuarine deposits, including poorly-drained floodplain and inner-estuary clays (Fig. 5). Based on the micropaleontological record, the transition from continental to inner-estuarine conditions is constrained between 9.5 and 8.9 cal kyr BP. Locally, near the southern PV flank, well-drained deposits laterally grade into poorly-drained floodplain sediments (Fig. 5). Between ~8.3 and 8.2 cal kyr BP, the inner estuarine succession becomes markedly organic-rich, marking the onset of the $S1break_{eq}$ interval (Fig. 5). Inner estuarine conditions persisted until approximately 8.2 cal kyr BP (Fig. 5).

The uppermost portion of the Lower Holocene succession is characterized by laterally extensive outer estuary deposits dated between 8.2 and 8.0 cal kyr BP (Fig. 5). Within the upper part of the $S1break_{eq}$ interval, these deposits are locally interrupted by crevasse channel bodies recognized along the paleovalley profile (cores It 12, T1, It 23; Fig. 5). Above the crevasse deposits, micropaleontological assemblages document the re-establishment of brackish outer-estuarine conditions, marking the transition to the overlying $S1b_{eq}$ interval (Fig. 5).

In the southern sector of the paleovalley, outer-estuary deposits are overlain by a channel-belt sand body extending between cores It18 and It25 (Fig. 5). This sand body exceeds 500 m in width, reaches a maximum thickness of approximately 5 m, and is chronologically constrained between ~8.0 and 5.6 cal kyr BP (Fig. 5).

Overall, the upper ~12 m of the Middle-Upper Holocene PVF (last ~8 kyr) records a shallowing-upward succession from estuarine clays to delta-plain (distributary channel) and poorly-drained floodplain deposits, capped by well-drained floodplain and fluvial-channel facies (Fig. 5). Paleoecological data constrain the transition from deepening-to shallowing-upward conditions to approximately 8.1 cal kyr BP. This transition defines the maximum flooding surface (MFS) within the Biferno paleovalley fill (Fig. 5). The MFS occurs within an interval characterized by the strongest marine influence, here referred to as the maximum flooding zone (MFZ). The corresponding interval is characterized by fine-grained outer-estuary deposits consistent with reduced fluvial energy and the maximum landward extent of marine influence during the Holocene transgression.

4.3. Geochemical characterization of sapropel S1-equivalent deposits

Facies analysis on the S1-equivalent interval ($S1_{eq}$; ~10.0-6.8 cal kyr BP) was integrated with bulk geochemical data shown in Table 3, including total nitrogen (TN), total organic carbon (TOC), and stable isotope compositions ($\delta^{13}C$ and $\delta^{15}N$). The resulting dataset documents the vertical distribution of these proxies throughout the S1-equivalent succession and provides the basis for comparing their variability among depositional facies and stratigraphic intervals (Fig. 6).

In general, TOC and TN concentrations display broadly similar vertical trends throughout the cored succession, whereas the $\delta^{13}C$ and $\delta^{15}N$ profiles exhibit opposite trends (Fig. 6). Mean values of all geochemical proxies were calculated for the three facies associations composing the $S1_{eq}$ succession (poorly drained floodplain, Pdf; inner estuary/swamp, IE/Sw; and outer estuary/lagoon, OE/L) and are reported in Table 4. Mean values were also calculated separately for $S1a_{eq}$, $S1break_{eq}$, and $S1b_{eq}$ intervals, as well as for each facies association (FA) within these intervals, allowing comparison of geochemical characteristics among depositional environments and through the $S1_{eq}$ succession.

5. Discussion

5.1. Onshore-offshore analysis

The high-resolution sedimentological, paleoecological, geochemical, and chronological framework developed for the Biferno paleovalley enables direct comparison of the terrestrial record with the coeval

Table 3
– Depths and analytical dataset of T1 core samples used for elemental (TOC and TN) and stable isotope ($\delta^{13}C$ and $\delta^{15}N$) analyses.

Sample	N_{tot}	TOC	$\delta^{13}C$	$\delta^{15}N$	C/N	Sample	N_{tot}	TOC	$\delta^{13}C$	δ^{15N}	C/N
Depth (m)	(%)	(%)	(‰)	(‰)		Depth (m)	(%)	(%)	(‰)	(‰)	
9.5	0.04	0.4	−25.0	5.1	9.5	18.4	0.10	1.8	−26.8	5.0	16.9
9.65	0.07	0.7	−20.7	5.0	10.6	18.8	0.20	2.6	−26.8	3.4	13.2
9.85	0.05	0.6	−23.4	4.7	11.1	18.95	0.10	0.6	−26.6	1.5	6.1
9.95	0.04	0.5	−24.8	4.3	11.3	19.15	0.11	0.8	−26.9	2.1	7.8
10.2	0.05	0.5	−25.8	5.8	9.5	19.4	0.13	1.4	−27.5	3.3	10.4
10.6	0.08	0.9	−21.1	4.9	10.7	19.8	0.11	2.6	−27.3	3.5	24.2
10.8	0.04	0.5	−24.3	5.8	11.4	20.15	0.09	0.9	−26.9	2.1	9.2
10.95	0.04	0.4	−25.7	5.0	11.6	20.5	0.09	0.5	−26.4	1.7	5.9
11.2	0.07	1.0	−25.2	5.2	13.5	20.8	0.09	0.5	−26.2	3.0	5.4
11.4	0.04	0.4	−25.8	6.9	8.7	20.9	0.09	0.4	−25.8	2.1	4.8
11.7	0.05	0.4	−25.3	7.1	8.9	21.15	0.10	0.6	−26.4	1.2	6.0
11.9	0.04	0.5	−26.0	8.1	12.0	21.5	0.08	0.6	−26.1	4.4	7.8
13.25	0.09	0.9	−20.5	5.0	9.6	21.8	0.07	0.5	−26.1	3.6	6.7
13.4	0.08	0.8	−20.5	4.8	9.9	22.15	0.07	0.4	−26.0	3.6	5.8
13.95	0.08	0.7	−21.0	5.6	8.7	22.45	0.07	0.5	−25.8	3.6	6.7
14.2	0.09	0.7	−21.5	5.3	8.3	22.65	0.08	0.7	−26.2	4.3	8.9
14.55	0.05	0.5	−26.0	7.0	9.6	23.45	0.07	0.4	−26.1	3.2	5.9
14.75	0.07	0.6	−23.0	5.6	9.2	23.65	0.07	0.5	−26.4	4.4	7.4
14.95	0.09	0.7	−25.2	6.5	8.1	24.2	0.10	1.0	−26.7	3.8	9.6
15.9	0.08	0.5	−25.2	6.7	6.8	24.45	0.07	0.6	−26.6	4.1	8.9
16.25	0.07	0.7	−24.1	5.8	9.5	24.55	0.11	1.1	−27.0	3.9	9.7
16.5	0.11	1.6	−27.5	4.8	14.3	24.65	0.12	1.0	−27.2	3.9	8.0
16.8	0.09	1.0	−26.7	7.7	10.8	24.75	0.11	0.7	−26.9	4.4	6.6
16.95	0.07	0.7	−24.0	5.4	9.4	24.85	0.09	0.5	−26.4	5.0	6.0
17.23	0.08	0.7	−26.6	7.2	9.4	24.95	0.07	0.3	−26.3	3.6	5.0
17.6	0.06	0.6	−23.2	5.8	10.0	26.85	0.07	0.6	−26.8	3.6	9.5
17.8	0.06	0.5	−26.2	7.9	9.3	28.4	0.07	0.5	−26.7	3.5	7.2
18.15	0.08	0.7	−23.9	6.7	8.1	28.55	0.07	0.6	−26.9	3.7	8.0

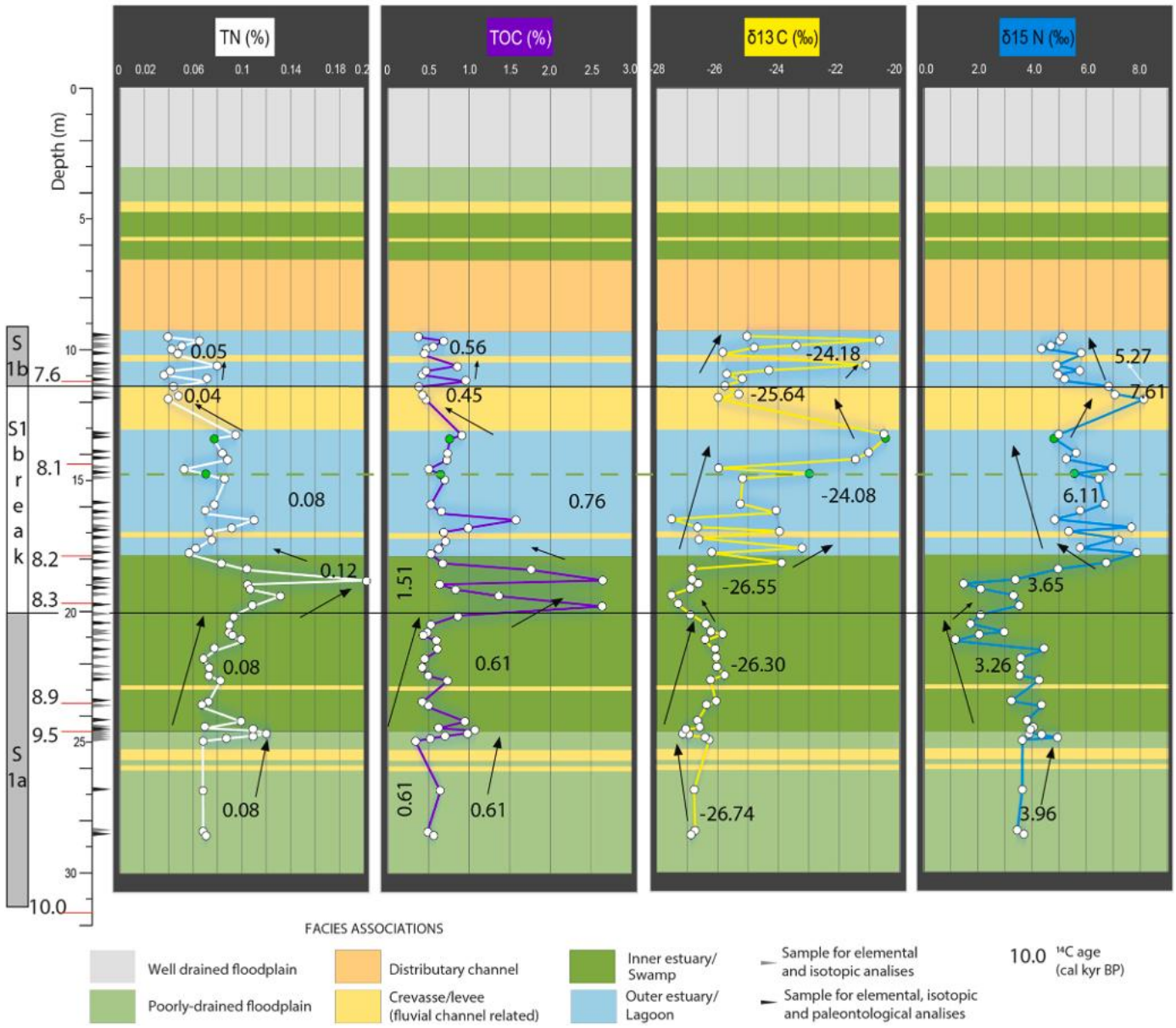

Fig. 6. – Integration of facies associations and geochemical data. Vertical distribution of bulk geochemical proxies (TN: total nitrogen; TOC: total organic carbon) and stable isotopes compositions ($\delta^{13}C$ and $\delta^{15}N$) from T1 core, framed within the facies architecture of the S1-equivalent interval. $S1a_{eq}$: S1a equivalent interval; $S1break_{eq}$: S1 break equivalent interval; $S1b_{eq}$: S1b equivalent interval.

Table 4
– Mean TOC, TN, $\delta^{13}C$, and $\delta^{15}N$ values calculated for the three facies associations recognized within the $S1_{eq}$ succession and for the individual $S1a_{eq}$, S1 $break_{eq}$, and $S1b_{eq}$ intervals. Pdf: poorly-drained floodplain; IE/Sw: Inner estuary/Swamp; OE/L: Outer estuary/Lagoon; FA: facies association.

		TN (%)	TOC (%)	$\delta^{13}C$ (‰)	δ15N (‰)
Mean FA values	Pdf	0.08	0.61	−26.74	3.96
	IE/Sw	0.10	0.90	−26.38	3.39
	OE/L	0.07	0.68	−24.12	5.76
$S1a_{eq}$	Pdf	0.08	0.61	−26.74	3.96
	IE/Sw	0.08	0.61	−26.30	3.26
	OE/L	-	-	-	-
S1 $break_{eq}$	IE/Sw	0.12	1.51	−26.55	3.65
	OE/L	0.08	0.76	−24.08	6.11
$S1b_{eq}$	IE/Sw	-	-	-	-
	OE/L	0.05	0.56	−24.18	5.27

offshore stratigraphic architecture of the Adriatic shelf (Fig. 7). Building upon the regional reconstruction proposed by Campo et al. (2024), the coastal plain-to-shelf correlation presented here is refined through the integration of the new T1 core, which provides improved chronological control together with the detailed facies architecture, paleoecological dataset, and geochemical characterization presented in this study. This integrated framework provides the basis for assessing how the evolution of the Biferno paleovalley fill relates to relative sea-level changes, coastal environmental evolution, and the timing of Sapropel S1 deposition. Within this framework, the $\delta^{13}C$ record provides an additional line of evidence for environmental reconstruction and stratigraphic correlation. Carbon isotopes have been widely employed in coastal settings to investigate relative sea-level changes and associated environmental transitions (Wilson et al., 2024). Although bulk-sediment stable isotopes and elemental geochemistry may have limitations when considered independently (e.g., Kemp et al., 2010), their integration with detailed facies, paleoecological, and chronological data

provides a robust basis for stratigraphic correlation and environmental reconstruction (Cloern et al., 2002; Kemp et al., 2013). Moreover, the overall correspondence between the $\delta^{13}C$ and $\delta^{15}N$ curves throughout the T1 succession (Fig. 6) further supports the interpretation of variations in organic matter sources and depositional conditions.

5.1.1. The onshore S1-equivalent ($S1_{eq}$)

Bulk-sediment samples from the $S1_{eq}$ interval of core T1, corresponding to the terrestrial counterpart of Sapropel S1, display a wide range of $\delta^{13}C$ values (−20.47‰ to −27.52‰; Figs. 6 and 7; Table 3). This variability demonstrates that depositional environments exerted a primary control on the isotopic composition of bulk organic matter throughout the $S1_{eq}$ succession and closely mirrors the vertical distribution of facies associations (Fig. 7).

The $S1a_{eq}$ interval, chronologically constrained between ~10.0 and 8.3 cal kyr BP (Fig. 7), is characterized by relatively limited $\delta^{13}C$ variability (−27.16‰ to −25.77‰) and is largely composed of poorly-drained floodplain deposits in its lower interval and inner estuarine deposits in its upper part (Fig. 7). Minor isotopic fluctuations occur immediately below the transition from continental to estuarine deposits, which is independently constrained by paleoecological data to between ~9.5 and 8.9 cal kyr BP (Fig. 5). This transition likely records progressive marine ingression within the Biferno paleovalley and is consistent with accelerated sea-level rise around ~9.2 cal kyr BP documented for the Adriatic sector (Fig. 7; Lambeck et al., 2011; Vacchi et al., 2016) and other regions (Liu et al., 2004). Comparable flooding phases have been documented in other western Adriatic coastal plains (e.g., Pescara and Po Plain), suggesting a basin-scale response likely associated with the post-9.2 cal kyr BP Meltwater Pulse 1C (MWP-1C), which promoted the progressive landward migration of barrier-lagoon systems toward their present-day coastal position (Fig. 7).

The transition to the $S1break_{eq}$ interval (~8.3-7.6 cal kyr BP) is marked by a pronounced decrease in $\delta^{13}C$ values (down to −27.52‰), coinciding with an abrupt increase in TOC within inner estuarine deposits (Figs. 6 and 7). Together, these trends suggest enhanced preservation and accumulation of predominantly terrigenous organic matter under restricted inner-estuary conditions. The overall behavior of the $\delta^{15}N$ record, which broadly shows an opposite trend to $\delta^{13}C$ throughout much of the succession (Fig. 6), provides additional support for this interpretation. The more depleted $\delta^{13}C$ values fall within the typical isotopic range of C3-derived organic matter (Fry and Sherr, 1984), consistent with the dominant terrestrial organic matter sources documented along the western Adriatic sector (Maselli et al., 2014; Pellegrini et al., 2021; Tesi et al., 2007). A comparable lithofacies shift towards highly organic-rich peaty clays has previously been documented within the Po Plain (EM2 core; Fig. 8), where it has been interpreted as

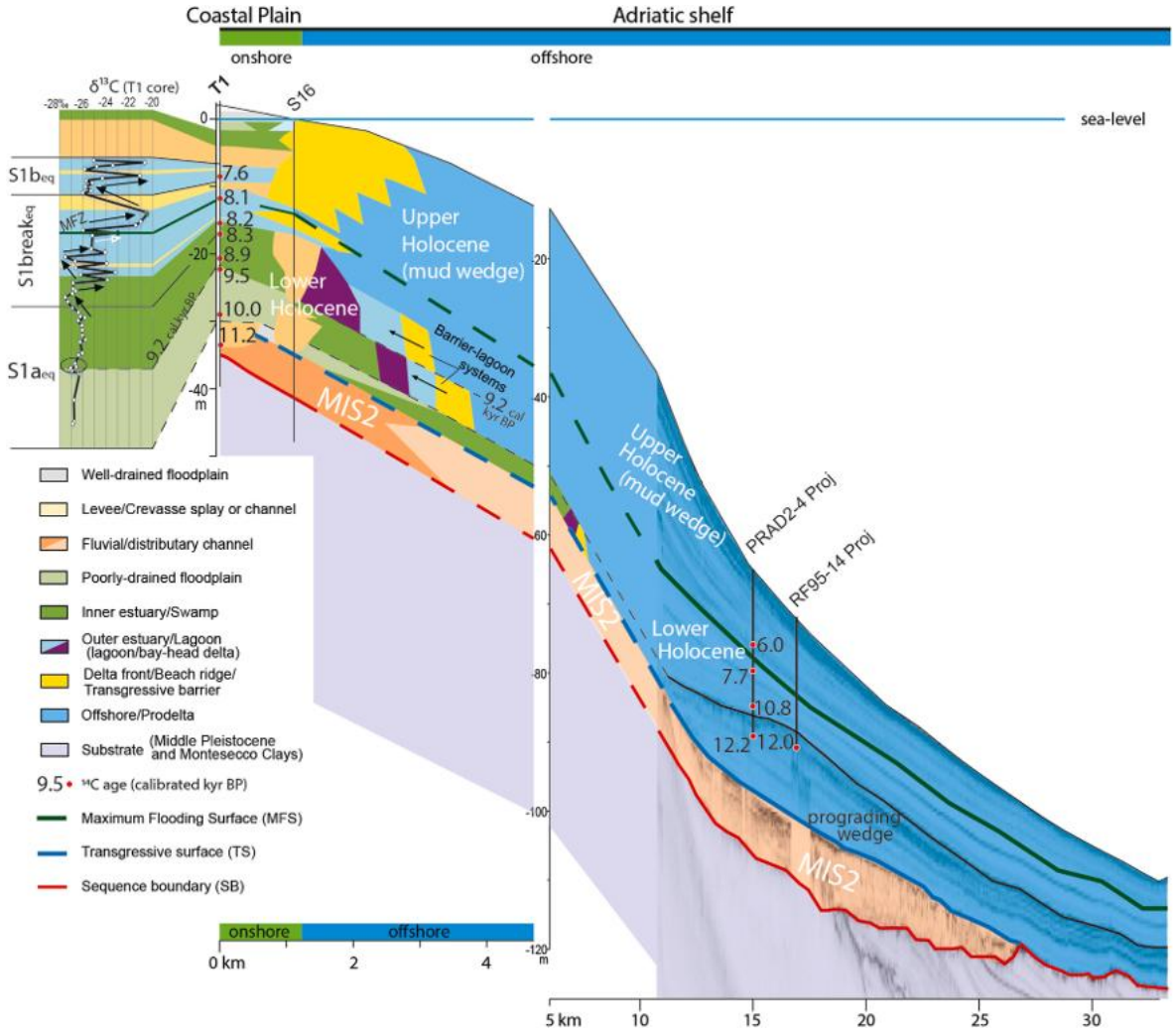

Fig. 7. – Onshore-offshore stratal architecture of the Biferno sector. Coastal-to-shelf stratigraphic framework extending from the T1 core (onshore-S1 equivalent succession) to the central Adriatic shelf (modified after Campo et al., 2024) and updated with the new chronostratigraphic, sedimentological and geochemical data presented in this study. The $\delta^{13}C$ profile from core T1 core is shown on the left, together with the distribution of samples analyzed for bulk geochemistry (white dots). MFZ: maximum flooding zone.

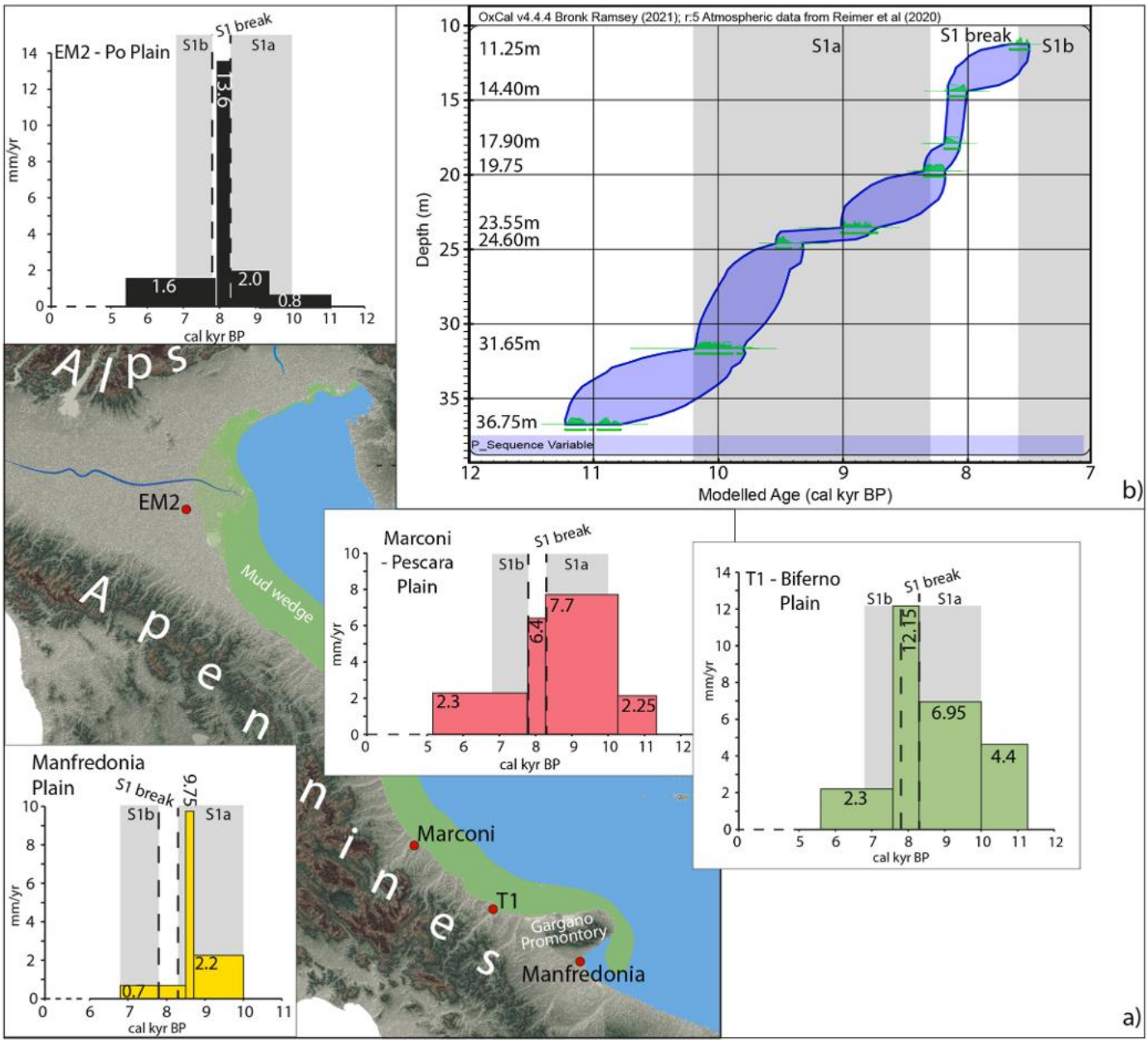

Fig. 8. Sedimentation rates across western Adriatic coastal paleovalley systems. a) Sediment accumulation rates calculated for four coastal plain records along the western Adriatic sector. Histograms summarize the rates estimated for the main S1 intervals (S1a, S1 break, and S1b) within terrestrial cored successions. b) Bayesian age-depth model of the reference T1 core used to constrain sediment accumulation rates.

reflecting progressive coastal flooding during the Early Holocene transgression (Amorosi et al., 2021). The occurrence of comparable sedimentological and geochemical signatures in geographically distinct paleovalley systems suggests that the onset of the S1break$_{eq}$ reflects a regional environmental reorganization rather than an isolated local process.

Within the S1break$_{eq}$ interval, the pronounced variability of the $\delta^{13}C$ record closely parallels repeated facies changes (Fig. 7), indicating rapid alternations between stronger terrestrial and marine influence within the evolving estuary. A marked positive shift in $\delta^{13}C$ (up to −23.23‰) accompanies the transition from inner-to outer estuarine deposits shortly after 8.2 cal kyr BP (Fig. 7), and suggests enhanced marine influence consistent with the post-8.2 kyr BP sea-level rise (Lambeck et al., 2014), likely associated with MWP-1D (Liu et al., 2004). The contemporaneous decrease in $\delta^{15}N$ values provides further support for this interpretation (Fig. 6). Conversely, the subsequent decrease in $\delta^{13}C$ values between 8.2 and 8.1 cal kyr BP coincides with the deposition of crevasse-channel deposits, suggesting renewed fluvial influence associated with river avulsion within the Biferno PVS.

The major flooding event at approximately 8.1 cal kyr BP, recorded by the accumulation of laterally extensive outer-estuary deposits (Fig. 5), marks the phase of maximum marine influence within the Biferno paleovalley system. This interpretation is primarily supported by the integrated facies, sedimentological and paleoecological framework, which documents the establishment of the least-confined estuarine conditions and the maximum landward extent of lagoonal environments. This interval is accompanied by a rapid increase in $\delta^{13}C$ values (from −27.50‰ to −24.07‰; Fig. 7), followed by a progressive upward enrichment within the overlying outer-estuary deposits (white arrow in Fig. 7). This least negative $\delta^{13}C$ value of the entire succession (−20.47‰ at 13.4 m core depth), together with the corresponding decrease in $\delta^{15}N$ values (Fig. 6), is consistent with an increased

contribution of marine-derived organic matter during the phase of maximum flooding. Although the isotopic and paleontological signals do not perfectly coincide stratigraphically, their overall agreement provides complementary evidence supporting the paleoenvironmental reconstruction. The same interval also coincides with the lowest pocket penetrometer values recorded throughout the T1 succession (Fig. 3), reflecting the accumulation of very soft, water-rich estuarine muds. Although pocket penetrometer measurements cannot be directly related to grain-size variations, their link with sedimentary facies changes and isotopic trends provides additional support for the interpretation of the maximum flooding zone (MFZ) at ~8.1 cal kyr BP.

Above the MFZ, between ~8.1 and 7.6 cal kyr BP, progressively decreasing $\delta^{13}C$ values (down to −25.99‰) coincide with the deposition of crevasse-channel deposits, indicating renewed fluvial influence following the maximum flooding phase, at the end of S1break$_{eq}$ (Fig. 7), as also documented by Maselli et al. (2014) for the Manfredonia PVS. The concomitant increase in $\delta^{15}N$ values (Fig. 6) provides additional support for this interpretation. Upsection, the basal S1b$_{eq}$ interval records the re-establishment of outer-estuary conditions. Although $\delta^{13}C$ values gradually become less negative upward, they remain consistently lower than those recorded within the MFZ, suggesting that marine influence was re-established but did not reach the degree observed during maximum flooding. This interpretation is consistent with the oligotypic meiofaunal assemblages described by Rossi et al. (2024), which indicate localized exchange with open-marine waters. The limited lateral extent of the outer-estuary deposits (Fig. 5), together with the occurrence of repeated fluvial avulsions and channel-belt deposition (Figs. 5 and 7), points to persistently unstable depositional conditions within the Biferno paleovalley during the final stages of post-glacial sea-level rise. The uppermost negative shift in $\delta^{13}C$ immediately below the crevasse deposits is interpreted as recording a renewed increase in terrestrial organic matter input associated with river avulsion prior to the transition towards Middle-Holocene delta-plain conditions.

5.1.2. *Coastal-to-shelf analysis of the S1$_{eq}$ interval*

In the western central Adriatic, the terrestrial S1$_{eq}$ is preferentially preserved within PVSs (Fig. 2c and 5). Fluvial channel bodies preserved beneath the modern Biferno coastal plain (T1 core; Fig. 7), chronologically constrained between the Younger Dryas (YD) and the earliest phases of post-glacial sea-level rise, likely fed the prominent offshore prograding wedge on the shelf (Fig. 7). New chronological constraints from the basal fluvial gravel body suggest that substantial riverine activity persisted after the YD. Combined with the age range documented for the offshore prograding wedge, this evidence further suggests that enhanced fluvial activity may have continued during the sea-level rise associated with MWP-1B (Lambeck et al., 2014). This source-to-sink relationship is consistent with sustained sediment flux during the melting phase at the end of the YD cold event (Pellegrini et al., 2016) and the earliest phase of postglacial sea-level rise. This configuration suggests enhanced transport of terrestrial sediment and freshwater to the basin immediately prior to the onset of S1 deposition. From a source-to-sink perspective, increased terrigenous supply may have contributed to reduced ventilation in the deepest sectors of the Adriatic. In line with this interpretation, grain-size records from the South Adriatic slope indicate a decrease in bottom-current energy since the end of the YD (Tesi et al., 2017), consistent with a progressive weakening of deep-water ventilation before the onset of S1.

Off the Biferno coast, Lower Holocene marine muds (~10.8-7.0 cal kyr BP) overlie the prominent prograding wedge (Fig. 7), documenting the rapid drowning of the Adriatic shelf during the Early-to-Mid Holocene transgressive phase. These marine deposits have a clear onshore counterpart in poorly-drained floodplain and estuarine sediments preserved within the Biferno PVF, encompassing the S1a$_{eq}$ and S1break$_{eq}$ intervals (Fig. 7). The rapid sea-level rise following MWP-1B (from ~60 to ~40 m b.s.l. in ~300 years; Lambeck et al., 2014) likely favored widespread drowning and erosion of coastal wetlands and estuarine environments, consistent with previous reconstructions from the northern Adriatic (Amorosi et al., 2016b; Correggiari et al., 1996; Storms et al., 2008) and the central Adriatic shelf (Pellegrini et al., 2015), possibly increasing the transfer of terrestrial organic matter towards the adjacent shelf and deeper sectors of the basin. Under these conditions, terrestrial and freshwater inputs were probably redistributed by waves and alongshore coastal currents (Fig. 2b), which likely displayed a wave-height field and southward-directed alongshore flow broadly comparable to the present-day (Pellegrini et al., 2015). This redistribution may have contributed to the organic-rich sedimentation observed in the deepest sectors of the basin (MAD and SAD) at the onset of the Adriatic S1 (~10.2 cal kyr BP). Although the relative contribution of this terrigenous supply and wetland drowning to S1 formation falls beyond the main scope of this study, these processes may represent additional, yet underexplored, concurrent factors in the development of S1 deposition.

At onshore locations, the progressive increase in $\delta^{13}C$ values reflects the landward migration of barrier-lagoon systems following the post-9.2 and post-8.2 kyr sea-level rise (Fig. 7), consistent with the MWP-1C and 1D flooding events. Upsection, the least negative $\delta^{13}C$ values are recorded at ~8.1 cal kyr BP, supporting the paleontological evidence for the MFZ, which marks the maximum landward extent of marine influence within the Biferno estuary during the S1 break.

Offshore, the corresponding interval is characterized by condensed deposition and coincides with a prominent downlap surface at the top of Lower-Holocene deposits (Fig. 7). The occurrence of repeated river avulsions towards the end of the S1break$_{eq}$ indicates renewed fluvial activity following the establishment of the MFZ and marks the onset of coastal progradation (Fig. 7). Enhanced riverine sediment supply during the S1b$_{eq}$ is consistent with the concurrent bayhead deltas progradation (Amorosi et al., 2017; Maselli et al., 2014) and the progressive accumulation of the Middle-Upper Holocene mud wedge along the Adriatic coastline (Fig. 7; Cattaneo et al., 2003), linking paleovalley infill processes with basin-scale sediment dispersal. Notably, S1b deposition predates the formation of the Adriatic mud wedge (>7.0 cal kyr BP; Fig. 7). This stratigraphic evidence suggests that increased sediment supply from western Adriatic rivers accompanied the transition from transgressive to highstand conditions, while sapropel deposition was still ongoing in the deepest sectors of the Adriatic (Tesi et al., 2017), further highlighting the temporal link between coastal sedimentary processes and basin-scale environmental evolution.

5.2. *Climatic forcing on S1 and riverine freshwater discharge: insights from S1$_{eq}$*

Sediment accumulation rates from the T1 core were compared with three coastal-plain records from the western Adriatic margin to assess the regional role of terrestrial systems during Sapropel S1 deposition (Fig. 8a). The four successions, recovered from three coastal plains north of the Gargano Promontory (Biferno, Pescara and Po) and one to the south (Manfredonia; Fig. 8a), represent paleovalley systems fed by rivers with contrasting drainage-basin size, lithological characteristics and sediment supply, thus providing a suitable framework to evaluate regional climatic signals against local source-to-sink variability. The cored successions are supported by robust chronostratigraphic and high-resolution facies frameworks (Amorosi et al., 2023; Bruno et al., 2017; Campo et al., 2022), with the EM2 record further constrained by pollen data providing independent climatic information (Cacciari et al., 2020). Among the four records, T1 provides the chronological reference framework through a Bayesian age-depth model constrained by eight radiocarbon ages (Fig. 8b). For the S1 interval (e.g., ~10.2-6.8 cal kyr BP), the resulting model highlights three main phases of sediment accumulation that closely match the sedimentation-rate histogram, with no significant chronological outliers detected (Fig. 8a and b).

Regardless of their geographic position, the EM2 and T1 records display remarkably similar sedimentation patterns, with relatively low

sedimentation rates during S1a (EM2 = 2.0 mm/yr; T1 = 6.95 mm/yr), a pronounced increase during the S1 break (EM2 = 13.6 mm/yr; T1 = 12.15 mm/yr), and minimum rates during S1b (EM2 = 1.6 mm/yr; T1 = 2.3 mm/yr; Fig. 8a). The Manfredonia core exhibits a broadly comparable trend, although its highest sedimentation rate occurs during the terminal phase of S1a (9.75 mm/yr; Fig. 8a). This difference likely reflects the more distal position of the core within the paleovalley system, where the succession may record stratigraphic condensation in proximity to the MFS. In contrast, the Marconi core records its highest accumulation rates during S1a (7.7 mm/yr), followed by lower values during the S1 break (6.4 mm/yr) and minimum rates during S1b (2.3 mm/yr; Fig. 8a). Similar low sedimentation rates during S1b are also documented in the Po and Biferno coastal plains (Amorosi et al., 2017), indicating a regional decrease in accumulation rates at landward sites during the Middle-Late Holocene. Despite these local differences, all four records document a substantial reduction in sediment accumulation during S1b, suggesting a regional decrease in accommodation within western Adriatic paleovalleys during the Middle-Late Holocene. Local variability among individual records is plausibly related to the relative position of the cores within their respective PVSs (proximal vs. distal settings), differences in catchment lithology (siliciclastic vs. carbonate source areas), and local geomorphological or climatic controls. Despite these differences, the broadly consistent sedimentation trends observed across all four records suggest that regional climatic and sea-level forcing exerted a primary control on sediment accumulation within western Adriatic paleovalleys.

During the $S1a_{eq}$ interval, pollen data from the Po coastal plain indicate the establishment of relatively warm climatic conditions following the YD cold event (Cacciari et al., 2020). A peak in montane taxa at ~9.3 cal kyr BP documents a short-lived cooling phase consistent with the Boreal Oscillation (Rasmussen et al., 2014), followed by the expansion of mixed oak forests marking the onset of the Holocene Climatic Optimum. This climatic evolution is consistent with the stratigraphic framework documented in the Biferno PVF (Fig. 5) and with the coastal-to-shelf reconstruction proposed in this study, which records progressive estuarine expansion during the early Holocene transgression. Pollen and stratigraphic records from the Po Plain identified two subsequent phases of climatic deterioration (~8.3-8.0 and ~7.7 cal kyr BP) during the Early-Mid Holocene transition (Cacciari et al., 2020). Independent stratigraphic and chronological evidence from the Pescara and Biferno paleovalley systems indicates that these climatic perturbations were accompanied by synchronous changes in depositional architecture along the western Adriatic sector. The first interval coincides with the onset of the S1 break and the highest sedimentation rates recorded in both the Po and Biferno areas (Fig. 8a). Pollen assemblages indicate cooler and wetter conditions, interpreted as the regional expression of the 8.2 ka event, likely associated with strengthening of the Bora wind over the northern sector (Cacciari et al., 2020). The second phase, although less clearly defined in the EM2 pollen records, is supported by independent pollen evidence from the southern Adriatic and isotope ($\delta^{13}C$ and $\delta^{18}O$) reconstructions from speleothems in central Italy (Zanchetta et al., 2007), suggesting increased precipitation and lower temperatures (Combourieu-Nebout et al., 2013). This climatic framework is consistent with the timing of the S1 break in the Adriatic, which has been interpreted as reflecting a temporary recovery of deep-water ventilation, possibly associated with enhanced NAdDW formation (Tesi et al., 2017). We infer that increased precipitation likely enhanced catchments erosion and sediment delivery to the river network through intensified denudation and soil erosion linked to the 8.2 ka cold event. The rapid expansion of estuarine systems during the transgressive phase following MWP-1D likely promoted efficient trapping of these sediments within western Adriatic PVSs, thereby favoring sediment accumulation at onshore sites while limiting the amount of terrigenous material exported to the open Adriatic (Figs. 5 and 8a). Consequently, much of the sediment supplied by western Adriatic river systems may have been preferentially stored within these expanding estuarine depocenters, whereas only a limited fraction of freshwater and associated sediment reached the deepest sectors of the Adriatic basin. This interpretation is further supported by the coastal-to-shelf correlation (Fig. 7), which indicates that substantial riverine activity, accompanied by sustained basinward transport of freshwater and terrigenous sediment, persisted during the earliest stages of Holocene transgression before progressively shifting landward estuarine depocenters, and potentially influencing the environmental conditions under which Sapropel S1 developed.

The onshore-offshore distribution of organic matter (OM) shown in Fig. 9 is consistent with the coastal-to-shelf reconstruction (Fig. 7) and documents the progressive shift from sustained riverine delivery of freshwater and terrigenous sediment during the earliest Holocene transgression to increasing trapping of organic-rich sediments within estuarine paleovalleys during Sapropel S1 deposition. TOC data indicate relatively elevated values within the $S1a_{eq}$ interval at onshore sites in the Biferno PVS, with concentrations generally exceeding 0.5% (Fig. 9). Within the Biferno system, the highest TOC values occurred during the early phase of the S1 break (~8.3-8.2 cal kyr BP), immediately preceding the major flooding associated with the rapid sea-level rise that followed MWP-1D (Fig. 7). Coeval organic-rich deposits identified within other PVSs (Amorosi et al., 2023; Campo et al., 2024; Ricci Lucchi et al., 2006) suggest that similar environmental conditions affected a broader sector of the western Adriatic coast. In contrast, TOC records from the deepest sectors of the basin, including the Adriatic slope and the South Adriatic Depression (SAD), show a marked decrease during the S1 break, whereas relatively high TOC values persisted within the Mid Adriatic Depression (MAD - Fig. 9). This contrasting pattern likely reflects the progressive landward migration of river mouths during the rapid sea-level rise following MWP-1D, which shifted the principal entry points of terrestrial material further inland and accentuated the onshore-offshore differentiation in OC accumulation during the S1 break. At the same time, rapid transgression may also have contributed to modifications in bottom-water circulation patterns (Fig. 2b), potentially reducing ventilation efficiency within the MAD, where OC accumulation persisted throughout the S1 break (Tesi et al., 2017). The rapid creation of accommodation space during the late stages of the Early Holocene transgression (MWP-1D) thus likely had a dual effect: it promoted the accumulation of stratigraphically expanded and organic-rich

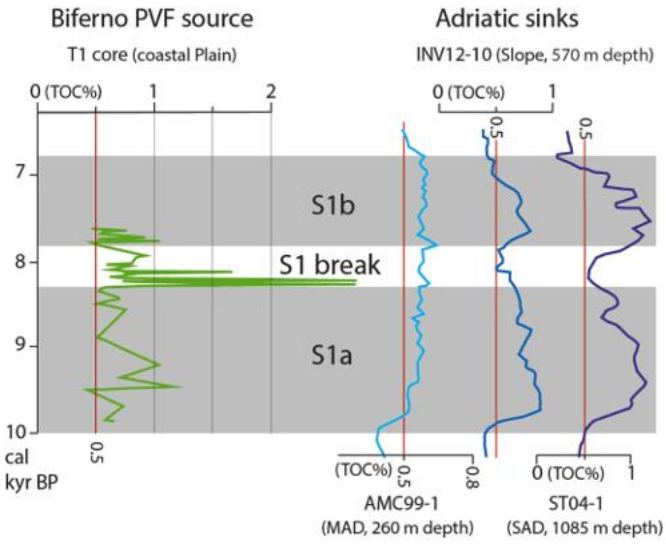

Fig. 9. – Onshore-offshore comparison of TOC accumulation during Sapropel S1 deposition in the Adriatic basin. TOC values from the S1-equivalent succession preserved within the Biferno paleovalley fill (PVF; T1 core) compared with coeval offshore records from the deepest sectors of the Adriatic basin (cores AMC99-1, ST04-1, and INV12-10; see Fig. 1b for locations). MAD: Mid Adriatic Depression. SAD: South Adriatic Depression.

onshore successions within PVSs while simultaneously inducing morphological and oceanographic changes at the basin scale that may have contributed to the partial recovery of deep-water ventilation during the S1 break. The subsequent phase of increased precipitation around ~7.7 cal kyr BP, together with renewed freshwater input, likely contributed to a renewed weakening of NAdDW formation, favoring S1b deposition. Independent records of precipitation anomalies from the northern and central Italian catchments between ~8.2 and 7.3 cal kyr BP (Spötl et al., 2010; Zanchetta et al., 2007) further support this interpretation. The final recovery of deep-water ventilation at ~6.8 cal kyr BP (Tesi et al., 2017) likely reflects the progressive establishment of more stable climatic-optimum conditions, coupled with mid-Holocene sea-level stabilization (Lambeck et al., 2014) and the weakening of North African monsoon precipitation (Weldeab et al., 2014).

5.3. Transient organic matter burial

A first-order assessment of the sediment volumes preserved within the western Adriatic paleovalley systems further supports the potential importance of these transient depocenters in the regional sediment budget. Although the available data do not allow a rigorous volumetric reconstruction, approximate calculations based on the reconstructed dimensions and thicknesses of the $S1a_{eq}$, $S1break_{eq}$ and $S1b_{eq}$ intervals within two well-documented Apennine systems (Biferno and Pescara) indicate individual sediment volumes of $< 1\,km^3$. These estimates should be regarded as order-of-magnitude values, given the simplifications in terms of paleovalley geometry, extent of deposits, and their landward migration during transgression. Nevertheless, the cumulative contribution of the approximately 30 Apennine catchments draining the western Adriatic margin (Amorosi et al., 2022) suggests that these relatively small individual depocenters may have represented an important component of the sediment temporarily stored within the PVSs along the western Adriatic margin. The Po Plain system represents a markedly larger sediment reservoir, with a first-order estimate of several tens of km^3 for the three S1eq intervals considered here. These values can be viewed in the broader source-to-sink framework of Amorosi et al. (2016b)), who estimated sediment volumes of ~200-235 km^3 for the continental shelf and ~60-85 km^3 for slope and basin for the whole TST. However, these estimates integrate a substantially longer interval (18-6 cal kyr BP) and therefore cannot be directly compared with the S1eq volumes calculated here. The marked stratigraphic expansion of transgressive (and highstand) deposits within paleovalleys is further supported by Campo et al. (2024), who documented cumulative TST + HST thicknesses of ~40 m in the Pescara paleovalley and ~30 m in the Biferno and Tronto systems, compared with <10 m above interfluves and at basinward offshore locations. Importantly, the TOC profiles shown in Fig. 9 indicate that organic-carbon concentrations within the Biferno PVS are of the same order of magnitude as those recorded in the Adriatic slope and basin settings, rather than being systematically higher. Given the much larger areal extent of offshore depositional domains, the available data do not support a direct equivalence between the carbon stored in paleovalleys and the reduction in offshore TOC concentrations. Nevertheless, the combination of comparable TOC concentrations, locally much greater stratigraphic thicknesses, and the multiplicity of western Adriatic paleovalley systems suggests that these coastal depocenters may have represented significant transient repositories of OC during Sapropel S1 deposition.

This first-order assessment supports the interpretation that rapid transgression promoted preferential sediment and organic-matter storage within coastal paleovalleys, while reducing the relative export of terrigenous material towards deeper Adriatic sectors.

6. Conclusion

This study provides new insights into the terrestrial record coeval with Mediterranean Sapropel S1 (~10.2-6.8 cal kyr BP) by integrating stratigraphic, sedimentological, geochemical, paleontological, and chronological data from the Biferno Paleovalley System (PVS), Southern Italy, within a source-to-sink perspective across the Adriatic basin.

The identification of the S1-equivalent succession ($S1a_{eq}$, $S1break_{eq}$, and $S1b_{eq}$) within core T1 demonstrates that paleovalley fills buried beneath modern coastal plains preserve continuous archives of Early to Mid-Holocene environmental change. The integration of sedimentological, paleoecological and geochemical proxies (TOC, TN, $\delta^{13}C$, $\delta^{15}N$) reveals a strong stratigraphic control on Organic Matter (OM) composition, with isotopic trends closely mirroring facies distribution and depositional conditions. In particular, the coupled but opposing behavior of $\delta^{13}C$ and $\delta^{15}N$ proved effective in tracking shifts between terrigenous and marine OM sources within Lower-Mid-Holocene estuarine deposits.

In T1 core, the $S1a_{eq}$ interval (~10.0-8.3 cal kyr BP) records predominantly poorly-drained floodplain to inner estuarine conditions, associated with relatively stable isotopic signatures. The transition to the $S1break_{eq}$ (~8.3-7.6 cal kyr BP) is marked by enhanced OM content and variability in both facies and geochemical proxies, reflecting high-frequency environmental instability during a phase of rapid sea-level rise and climatic perturbations. The overlying $S1b_{eq}$ interval documents renewed outer-estuarine conditions under increasingly unstable fluvial dynamics during the final stages of Holocene sea-level rise.

The onshore-offshore correlation highlights a spatial decoupling in OM accumulation during the S1 break, with enhanced terrigenous OM storage within PVSs and reduced export towards deeper basin sectors. This pattern reflects the progressive landward migration of river mouths during the Holocene transgression, which promoted the confinement of sediment, freshwater and organic matter within the expanding estuarine depocenters. Although the available data do not allow a direct assessment of fluvial influence on deep-water ventilation, these processes may have contributed to basin-scale environmental changes accompanying Sapropel S1 deposition.

At the regional scale, sediment accumulation rates and pollen data indicate a strong coupling between climatic variability, sea-level rise, and sediment supply. Increased precipitation and reduced vegetation cover during Early-Mid Holocene climatic perturbations (including the 8.2 ka event) likely enhanced sediment production and delivery to coastal systems, while estuarine environments acted as efficient sediment traps. Rapid accommodation-space creation during stepwise Holocene sea-level rise likely promoted the accumulation of thick organic-rich successions within PVSs and may also have contributed to broader morphological and oceanographic changes across the Adriatic basin.

First-order sediment-volume estimates indicate that individual Apennine paleovalley systems may have stored $< 1\,km^3$ of sediment during S1, whereas their cumulative contribution across the western Adriatic margin may have reached several km^3 and potentially tens of km^3. Despite the inherent uncertainties, these estimates, together with stratigraphic and TOC data, support the role of paleovalleys as transient sediment and organic-matter repositories during rapid transgression, without implying a direct quantitative equivalence between onshore carbon storage and offshore decreases in organic-carbon accumulation.

Overall, this study demonstrates that paleovalley fills represent a key yet previously underexplored component of the Adriatic source-to-sink system during Mediterranean Sapropel S1 deposition. Their exceptional stratigraphic continuity provides a unique terrestrial archive for reconstructing the transfer, storage and redistribution of sediment, freshwater and organic matter across the coastal-to-marine continuum. Integrating these onshore records with offshore stratigraphic successions offers a comprehensive framework for understanding the links between coastal evolution, sediment routing and basin-scale environmental change during Mediterranean Sapropel S1 deposition.

Author contributions

All authors made substantial contributions to this paper. Bruno Campo and Alessandro Amorosi planned the borehole drilling. Bruno Campo conceptualized the structure of the study, coordinated the manuscript preparation and wrote a substantial part of the text. Federico Purri carried out core sampling for paleoenvironmental (geochemical and microfossil) and chronological (14C) analyses and drafted the Geological Setting section under the supervision of Bruno Campo. Irene Altea De Vincenzo, under the supervision of Bruno Campo and Andrea Di Marino, produced the onshore stratigraphic cross-section (Fig. 5). Andrea Di Martino calibrated the radiocarbon dates, developed the Bayesian age-depth model, and wrote the corresponding section. Veronica Rossi and Stefano Claudio Vaiani contributed to the planning of microfossil sampling, performed paleontological analyses, and wrote the related section. Alessio Nogarotto coordinated laboratory activities for geochemical analyses and contributed to data interpretation under the supervision of Tommaso Tesi, who wrote the geochemistry section. Wan Hong provided 14C dates. Bruno Campo revised the paper that has been revised and edited by Claudio Pellegrini and Alessandro Amorosi.

Funding sources

This work was supported by the Italian Ministry of University and Research under the PRIN PNRR2022 program, project number P2022LMCW2, CLOSER: CLimate forcing On Adriatic SEa deoxygenation: A multi-archive Reconstruction of Sapropel S1, grant to Claudio Pellegrini.

Declaration of competing interests

The authors declare that they have no known competing financial interests or personal relationships that could have appeared to influence the work reported in this paper.

Acknowledgements

We thank Dr. Irene Albino ("Materiali Incoerenti" Laboratory - BiGeA, Università di Bologna) for her valuable support in sediment sample preparation. Her contribution was fundamental to the laboratory activities.

Appendix A. Supplementary data

Supplementary data to this article can be found online at https://doi.org/10.1016/j.quascirev.2026.110236.

Data availability

All data and/or code is contained within the submission.

References

Allen, G.P., Posamentier, H.W., 1993. Sequence stratigraphy and facies model of an incised valley fill: the Gironde Estuary, France. SEPM J. Sediment. Res. https://doi.org/10.1306/D4267B09-2B26-11D7-8648000102C1865D.

Amato, V., Aucelli, P., Bracone, V., Cesarano, M., Rosskopf, C., 2017. Long-term landscape evolution of the Molise sector of the central-southern apennines, Italy. Geol. Carpathica 68, 29–42. https://doi.org/10.1515/geoca-2017-0003.

Amorosi, A., Bracone, V., Campo, B., D'Amico, C., Rossi, V., Rosskopf, C.M., 2016a. A late Quaternary multiple paleovalley system from the Adriatic coastal plain (Biferno River, Southern Italy). Geomorphology 254, 146–159. https://doi.org/10.1016/j.geomorph.2015.11.023.

Amorosi, A., Bruno, L., Cacciari, M., Campo, B., Rossi, V., 2021. Tracing marine flooding surface equivalents across freshwater peats and other wetland deposits by integrated sedimentological and pollen data. Int. J. Coal Geol. 246, 103830. https://doi.org/10.1016/j.coal.2021.103830.

Amorosi, A., Bruno, L., Caldara, M., Campo, B., Cau, S., De Santis, V., Di Martino, A., Hong, W., Lucci, G., Pellegrini, C., Rossi, V., 2023. Late Quaternary sedimentary record of estuarine incised-valley filling and interfluve flooding: the Manfredonia paleovalley system (southern Italy). Mar. Pet. Geol. 147, 105975. https://doi.org/10.1016/j.marpetgeo.2022.105975.

Amorosi, A., Bruno, L., Campo, B., Morelli, A., 2015. The value of pocket penetration tests for the high-resolution palaeosol stratigraphy of late Quaternary deposits. Geol. J. 50, 670–682. https://doi.org/10.1002/gj.2585.

Amorosi, A., Bruno, L., Campo, B., Morelli, A., Rossi, V., Scarponi, D., Hong, W., Bohacs, K.M., Drexler, T.M., 2017. Global sea-level control on local parasequence architecture from the Holocene record of the Po plain, Italy. Mar. Pet. Geol. 87, 99–111. https://doi.org/10.1016/j.marpetgeo.2017.01.020.

Amorosi, A., Guermandi, M., Marchi, N., Sammartino, I., 2014. Fingerprinting sedimentary and soil units by their natural metal contents: a new approach to assess metal contamination. Sci. Total Environ. 500–501, 361–372. https://doi.org/10.1016/j.scitotenv.2014.08.078.

Amorosi, A., Lucchi, M.R., Rossi, V., Sarti, G., 2009. Climate change signature of small-scale parasequences from Lateglacial–Holocene transgressive deposits of the Arno valley fill. Palaeog. Palaeocl. Palaeoec. 273 (1–2), 142–152. https://doi.org/10.1016/j.palaeo.2008.12.010.

Amorosi, A., Marchi, N., 1999. High-resolution sequence stratigraphy from piezocone tests: an example from the late Quaternary deposits of the southeastern Po plain. Sediment. Geol. 128, 67–81. https://doi.org/10.1016/S0037-0738(99)00062-7.

Amorosi, A., Maselli, V., Trincardi, F., 2016b. Onshore to offshore anatomy of a late Quaternary source-to-sink system (po plain–adriatic sea, Italy). Earth Sci. Rev. 153, 212–237. https://doi.org/10.1016/j.earscirev.2015.10.010.

Amorosi, A., Sammartino, I., Dinelli, E., Campo, B., Guercia, T., Trincardi, F., Pellegrini, C., 2022. Provenance and sediment dispersal in the Po-Adriatic source-to-sink system unraveled by bulk-sediment geochemistry and its linkage to catchment geology. Earth Sci. Rev. 234, 104202. https://doi.org/10.1016/j.earscirev.2022.104202.

Artegiani, A., Paschini, E., Russo, A., Bregant, D., Raicich, F., Pinardi, N., 1997a. The adriatic sea general circulation. Part I: Air–Sea interactions and water mass structure. J. Phys. Oceanogr. 27 (2), 1492–1514. https://doi.org/10.1175/1520-0485(1997)027%3C1492:TASGCP%3E2.0.CO.

Artegiani, A., Paschini, E., Russo, A., Bregant, D., Raicich, F., Pinardi, N., 1997b. The adriatic Sea general circulation. Part II: baroclinic circulation structure. J. Phys. Oceanogr. 27 (2), 1515–1532. https://doi.org/10.1175/1520-0485(1997)027%3C1515:TASGCP%3E2.0.CO.

Athersuch, J., Horne, D.J., Whittaker, J.E., 1989. Marine and brackish water ostracods (Superfamilies cypridacea and Cytheracea): Keys and notes for the identification of the species. In: The Linnean Society of London & the Esturine and brackish-water Sciences Association. E.J. Brill.

Aucelli, P.P.C., Faillace, P.I., Rosskopf, C.M., 2009. Evoluzione geomorfologica del tratto finale del fondovalle del Fiume Biferno (Molise) dal 1800 ad oggi. Mem. Soc. Geol. Ital. 87, 367–378. https://hdl.handle.net/11695/15620.

Barbieri, G., Vaiani, S.C., 2018. Benthic Foraminifera or Ostracoda? Comparing the accuracy of palaeoenvironmental indicators from a Pleistocene lagoon of the Romagna coastal plain (Italy). J. Micropalaeontology 37, 203–230. https://doi.org/10.5194/jm-37-203-2018.

Bhattacharya, J.P., 2006. Deltas. In: Posamentier, H.W., Walker, R.G. (Eds.), Facies Models Revisited. SEPM Society for Sedimentary Geology, vol. 84. Special Publications, Tulsa (Oklahoma), pp. 237–292. https://doi.org/10.2110/pec.06.84.0237.

Bhattacharya, J.P., 2011. Practical problems in the application of the sequence stratigraphic method and key surfaces: integrating observations from ancient fluvial–deltaic wedges with Quaternary and modelling studies. Sedimentology 58 (1), 120–169. https://doi.org/10.1111/j.1365-3091.2010.01205.x.

Blum, M.D., 1993. Genesis and architecture of incised valley fill sequences: a late Quaternary example from the Colorado river, gulf coastal plain of Texas. In: Weimer, P., Posamentier, H. (Eds.), Siliciclastic Sequence Stratigraphy: Recent Developments and Applications. American Association of Petroleum Geologists. https://doi.org/10.1306/M58581C10.

Blum, M.D., 2007. Large river systems and climate change. In: Gupta, A. (Ed.), Large Rivers: Geomorphology and Management. John Wiley and Sons, Chichester, UK, pp. 627–659. https://doi.org/10.1002/9781119412632.ch32.

Blum, M.D., Aslan, A., 2006. Signatures of climate vs. sea-level change within incised valley-fill successions: quaternary examples from the Texas GULF Coast. Sediment. Geol. 190, 177–211. https://doi.org/10.1016/j.sedgeo.2006.05.024.

Blum, M.D., Martin, J., Milliken, K., Garvin, M., 2013. Paleovalley systems: insights from Quaternary analogs and experiments. Earth Sci. Rev. 116, 128–169. https://doi.org/10.1016/j.earscirev.2012.09.003.

Blum, M.D., Törnqvist, T., 2000. Fluvial responses to climate and sea-level change: a review and look forward. Sedimentology 47, 2–48. https://doi.org/10.1046/j.1365-3091.2000.00008.x.

Boldrin, A., Langone, L., Miserocchi, S., Turchetto, M., Acri, F., 2005. Po river plume on the Adriatic continental shelf: dispersion and sedimentation of dissolved and suspended matter during different river discharge rates. Mar. Geol. 222–223, 135–158. https://doi.org/10.1016/j.margeo.2005.06.010.

Bonaduce, G., Ciampo, G., Masoli, M., 1975. Distribution of ostracoda in the adriatic sea. Pubbl. Stn. Zool. Napoli 40, 1–304.

Bonaldo, D., Benetazzo, A., Bergamasco, A., Campiani, E., Foglini, F., Sclavo, M., Trincardi, F., Carniel, S., 2016. Interactions among Adriatic continental margin morphology, deep circulation and bedform patterns. Mar. Geol. 375, 82–98. https://doi.org/10.1016/j.margeo.2015.09.012.

Boyd, R., Dalrymple, R.W., Zaitlin, B.A., 2006. Estuarine and incised-valley facies models. In: Posamentier, H.W., Walker, R.G. (Eds.), Facies Models Revisited, vol. 84. SEPM Society for Sedimentary Geology, pp. 171–235. https://doi.org/10.2110/pec.06.84.0171.

Bracone, V., Amorosi, A., Aucelli, P.P.C., Rosskopf, C.M., Scarciglia, F., Di Donato, V., Esposito, P., 2011. The Pleistocene tectono--sedimentary evolution of the Apenninic foreland basin between Trigno and Fortore rivers (Southern Italy) through a sequence-stratigraphic perspective. Basin Res. 24 (2), 213–233. https://doi.org/10.1111/j.1365-2117.2011.00523.x.

Bridge, J.S., 2006. Fluvial facies models: recent developments. In: Posamentier, H.W., Walker, R.G. (Eds.), Facies Models Revisited, vol. 84. SEPM Society for Sedimentary Geology, pp. 85–170. https://doi.org/10.2110/pec.06.84.0085.

Broecker, W.S., Denton, G.H., Edwards, R.L., Cheng, H., Alley, R.B., Putnam, A.E., 2010. Putting the younger dryas cold event into context. Quat. Sci. Rev. 29, 1078–1081. https://doi.org/10.1016/j.quascirev.2010.02.019.

Bruno, L., Bohacs, K.M., Campo, B., Drexler, T.M., Rossi, V., Sammartino, I., Scarponi, D., Hong, W., Amorosi, A., 2017. Early Holocene transgressive palaeogeography in the Po coastal plain (northern Italy). Sedimentology 64, 1792–1816. https://doi.org/10.1111/sed.12374.

Bruno, L., Campo, B., Martino, A.D., Hong, W., Amorosi, A., 2019. Peat layer accumulation and post-burial deformation during the mid-late Holocene in the Po coastal plain (Northern Italy). Basin Res. 31 (3), 621–639. https://doi.org/10.1111/bre.12339.

Cacciari, M., Amorosi, A., Marchesini, M., Kaniewski, D., Bruno, L., Campo, B., Rossi, V., 2020. Linking Holocene vegetation dynamics, palaeoclimate variability and depositional patterns in coastal successions: insights from the Po Delta plain of northern Italy. Palaeogeogr. Palaeoclimatol. Palaeoecol. 538, 109468. https://doi.org/10.1016/j.palaeo.2019.109468.

Campo, B., Barbieri, G., Di Martino, A., Hong, W., Scarponi, D., Vaiani, S.C., Amorosi, A., 2022. The Pescara Paleovalley system (Central Italy): a millennial-scale record of late Pleistocene and Holocene glacio-eustatic events. Mar. Pet. Geol. 145, 105908. https://doi.org/10.1016/j.marpetgeo.2022.105908.

Campo, B., Bruno, L., Amorosi, A., 2023. Sedimentary facies characterization through CPTU profiles: an effective tool for subsurface investigation of modern alluvial and coastal plains. Sedimentology 70 (4), 1302–1327. https://doi.org/10.1111/sed.13079.

Campo, B., Pellegrini, C., Sammartino, I., Trincardi, F., Amorosi, A., 2024. New perspectives on offshore groundwater exploration through integrated sequence-stratigraphy and source-to-sink analysis: insights from the late Quaternary succession of the western central Adriatic system, Italy. Earth Sci. Rev. 256, 104880. https://doi.org/10.1016/j.earscirev.2024.104880.

Canals, M., Danovaro, R., Heussner, S., Lykousis, V., Puig, P., Trincardi, F., Calafat, A.M., De Madron, X.D., Palanques, A., Sànchez-Vidal, A., 2009. Cascades in Mediterranean submarine grand canyons. Oceanography (Wash. D. C.) 22, 26–43.

Cattaneo, A., Correggiari, A., Langone, L., Trincardi, F., 2003. The late-Holocene Gargano subaqueous delta, adriatic shelf: sediment pathways and supply fluctuations. Mar. Geo. 193 (1–2), 61–91. https://doi.org/10.1016/S0025-3227(02)00614-X.

Cattaneo, A., Trincardi, F., 1999. The late Quaternary transgressive record in the Adriatic epicontinental sea: basin widening and facies partitioning. In: Bergman, K.M., Snedden, J.W. (Eds.), Isolated Shallow Marine Sand Bodies: Sequence Stratigraphic Analysis and Sedimentological Interpretation, vol. 64, pp. 127–146. https://doi.org/10.2110/pec.99.64.0127.

Cattaneo, A., Trincardi, F., Asioli, A., Correggiari, A., 2007. The Western Adriatic shelf clinoform: energy-limited bottomset. Cont. Shelf Res. 27, 506–525. https://doi.org/10.1016/j.csr.2006.11.013.

Chaumillon, E., Tessier, B., Reynaud, J.Y., 2010. Stratigraphic records and variability of incised valleys and estuaries along French coasts. Bull. Société Géologique Fr 181 (2), 75–85. https://doi.org/10.2113/gssgfbull.181.2.75.

Chiggiato, J., Bergamasco, A., Borghini, M., Falcieri, F.M., Falco, P., Langone, L., Miserocchi, S., Russo, A., Schroeder, K., 2016. Dense-water bottom currents in the Southern Adriatic sea in spring 2012. Mar. Geol. 375, 134–145. https://doi.org/10.1016/j.margeo.2015.09.005.

Cimerman, F., Langer, M.R., 1991. Mediterranean foraminifera. Academia Scientiarum et Artium Slovenica Classis IV 30.

Cloern, J.E., Canuel, E.A., Harris, D., 2002. Stable carbon and nitrogen isotope composition of aquatic and terrestrial plants of the San Francisco Bay estuarine system. Limnol. Oceanogr. 47, 713–729. https://doi.org/10.4319/lo.2002.47.3.0713.

Combourieu-Nebout, N., Peyron, O., Bout-Roumazeilles, V., Goring, S., Dormoy, I., Joannin, S., Sadori, L., Siani, G., Magny, M., 2013. Holocene vegetation and climate changes in the central Mediterranean inferred from a high-resolution marine pollen record (Adriatic sea). Clim. Past 9, 2023–2042. https://doi.org/10.5194/cp-9-2023-2013.

Correggiari, A., Roveri, M., Trincardi, F., 1996. Late Pleistocene and Holocene evolution of the north Adriatic sea. Alp. Mediterr. Quat. 9, 697–704.

Dalla Valle, G., Gamberi, F., Trincardi, F., Baglioni, L., Errera, A., Rocchini, P., 2013. Contrasting slope channel styles on a prograding mud-prone margin. Mar. Pet. Geol. 41, 72–82. https://doi.org/10.1016/j.marpetgeo.2012.02.003.

Dalrymple, R.W., 2006. Incised valleys in time and space: an introduction to the volume and an examination of the controls on valley formation and filling. In: Dalrymple, R. W., Leckie, D.A., Tillman, R.W. (Eds.), Incised Valleys in Time and Space. SEPM Society for Sedimentary Geology. https://doi.org/10.2110/pec.06.85.0005.

De Lange, G.J., Thomson, J., Reitz, A., Slomp, C.P., Speranza Principato, M., Erba, E., Corselli, C., 2008. Synchronous basin-wide formation and redox-controlled preservation of a Mediterranean sapropel. Nat. Geosci. 1, 606–610. https://doi.org/10.1038/ngeo283.

Di Martino, A., Sgattoni, G., Purri, F., Amorosi, A., 2024. Seismic amplification of late Quaternary paleovalley systems: 2D seismic response analysis of the Pescara paleovalley (Central Italy). Eng. Geol. 341, 107697. https://doi.org/10.1016/j.enggeo.2024.107697.

Drago, T., Freitas, C., Rocha, F., Moreno, J., Cachão, M., Naughton, F., Fradique, C., Araújo, F., Silveira, T., Oliveira, A., Cascalho, J., Fatela, F., 2006. Paleoenvironmental evolution of estuarine systems during the last 14000 years - the case of Douro Estuary (NW Portugal). J. Coast Res. 186–192.

Durand, M., Mojtahid, M., Maillet, G.M., Baltzer, A., Schmidt, S., Blet, S., Marchès, E., Howa, H., 2018. Late Holocene record from a Loire river incised paleovalley (French inner continental shelf): insights into regional and global forcing factors. Palaeogeogr. Palaeoclimatol. Palaeoecol. 511, 12–28. https://doi.org/10.1016/j.

Ellis, B.F., Messina, A.R., 1940. Catalogue of Foraminifera. Micropaleontology Press, New York, NY, USA.

Ellis, B.F., Messina, A.R., 1952. Catalogue of Ostracoda. The American Museum of Natural History. Special Publications, New York, NY, USA.

Ferrarini, F., Arrowsmith, J.R., Brozzetti, F., De Nardis, R., Cirillo, D., Whipple, K.X., Lavecchia, G., 2021. Late Quaternary tectonics along the Peri-Adriatic sector of the apenninic chain (Central-Southern Italy): inspecting active shortening through topographic relief and fluvial network analyses. Lithosphere 1–26. https://doi.org/10.2113/2021/7866617.

Fontana, A., Mozzi, P., Bondesan, A., 2008. Alluvial megafans in the Venetian–Friulian plain (north-eastern Italy): evidence of sedimentary and erosive phases during late Pleistocene and Holocene. Quat. Int. 189, 71–90. https://doi.org/10.1016/j.quaint.2007.08.044.

Fry, B., Sherr, E.B., 1984. d13C Measurements as Indicators of Carbon Flow in Marine and Freshwater Ecosystems, vol. 27, pp. 13–47.

Goodbred, S.L., Kuehl, S.A., Steckler, M.S., Sarker, M.H., 2003. Controls on facies distribution and stratigraphic preservation in the Ganges–Brahmaputra delta sequence. Sediment. Geol. 155, 301–316. https://doi.org/10.1016/S0037-0738(02)00184-7.

Grimm, R., Maier-Reimer, E., Mikolajewicz, U., Schmiedl, G., Müller-Navarra, K., Adloff, F., Grant, K.M., Ziegler, M., Lourens, L.J., Emeis, K.-C., 2015. Late glacial initiation of Holocene eastern Mediterranean sapropel formation. Nat. Commun. 6, 7099. https://doi.org/10.1038/ncomms8099.

Hayward, A., Wright, S.W., Carroll, D., Law, C.S., Wongpan, P., Gutiérrez-Rodriguez, A., Pinkerton, M.H., 2025. Antarctic phytoplankton communities restructure under shifting sea-ice regimes. Nat. Clim. Change 15, 889–896. https://doi.org/10.1038/s41558-025-02379-x.

Henderson, P.A., 1990. Freshwater ostracods. In: Kermack, D.M., Barnes, R.S.K. (Eds.), Synopses of the British Fauna (New Series), p. 228. Leiden, The Netherlands.

Hennekam, R., Jilbert, T., Schnetger, B., de Lange, G.J., 2014. Solar forcing of Nile discharge and sapropel S1 formation in the early to middle Holocene eastern Mediterranean. Paleoceanography 29, 343–356. https://doi.org/10.1002/2013PA002553.

Hilgen, F.J., 1991. Astronomical calibration of Gauss to Matuyama sapropels in the Mediterranean and implication for the Geomagnetic Polarity Time Scale. Earth Planet Sci. Lett. 104 (2–4), 226–244. https://doi.org/10.1016/0012-821X(91)90206-W.

Holbrook, J., Scott, R., Oboh-Ikuenobe, F., 2006. Base-level buffers and buttresses: a model for upstream versus downstream control on fluvial geometry and architecture within sequences. J. Sediment. Res. 76, 162–174. https://doi.org/10.2110/jsr.2005.10.

Horozal, S., Chae, S., Seo, J.M., Lee, S.M., Han, H.S., Cukur, D., Kim, E.D., Son, J.H., 2021. Quaternary evolution of the southeastern Korean continental shelf, East sea: paleo-incised valley and channel systems. Mar. Petrol. Geol. 128, 105011. https://doi.org/10.1016/j.marpetgeo.2021.105011.

Ishihara, T., Sugai, T., 2017. Eustatic and regional tectonic controls on late Pleistocene paleovalley morphology in the central Kanto Plain, Japan. Quat. Int. 456, 69–84. https://doi.org/10.1016/j.quaint.2017.06.029.

Jorissen, F.J., 1988. Benthic Foraminifera from the Adriatic sea; principles of phenotypic variation. Utrecht Micropaleontol. Bull. 37, 1–176.

Kemp, A.C., Horton, B.P., Vane, C.H., Bernhardt, C.E., Corbett, D.R., Engelhart, S.E., Anisfeld, S.C., Parnell, A.C., Cahill, N., 2013. Sea-level change during the last 2500 years in New Jersey, USA. Quat. Sci. Rev. 81, 90–104. https://doi.org/10.1016/j.quascirev.2013.09.024.

Kemp, A.C., Vane, C.H., Horton, B.P., Culver, S.J., 2010. Stable carbon isotopes as potential sea-level indicators in salt marshes, North Carolina, USA. Holocene 20 (4), 623–636. https://doi.org/10.1177/0959683609354302.

Kidd, R.B., Cita, M.B., Ryan, W.B.F., 1978. Stratigraphy of eastern Mediterranean sapropel sequences recovered during Leg 42A and their paleoenvironmental significance. Initial rep. Deep sea drill. Proj 42A, 421–443. https://doi.org/10.2973/dsdp.proc.42-1.113-1.1978.

Klein, B., Roether, W., Civitarese, G., Gacic, M., Manca, B.B., d'Alcala, M.R., 2000. Is the Adriatic returning to dominate the production of Eastern Mediterranean deep water? Geophys. Res. Lett. 27, 3377–3380. https://doi.org/10.1029/2000GL011620.

Lai, Z., Liu, Y., Wu, Z., Xu, Y., Fang, Z., Montgomery, D.R., 2025. Headward incision of large rivers in response to glacial sea level fall. Sci. Adv. 11. https://doi.org/10.1126/sciadv.adr5446 eadr5446.

Lambeck, K., Antonioli, F., Anzidei, M., Ferranti, L., Leoni, G., Scicchitano, G., Silenzi, S., 2011. Sea level change along the Italian coast during the Holocene and projections for the future. Quat. Int. 232, 250–257. https://doi.org/10.1016/j.quaint.2010.04.026.

Lambeck, K., Rouby, H., Purcell, A., Sun, Y., Sambridge, M., 2014. Sea level and global ice volumes from the last glacial maximum to the Holocene. Proc. Natl. Acad. Sci. 111, 15296–15303. https://doi.org/10.1073/pnas.1411762111.

Langone, L., Conese, I., Miserocchi, S., Boldrin, A., Bonaldo, D., Carniel, S., Chiggiato, J., Turchetto, M., Borghini, M., Tesi, T., 2016. Dynamics of particles along the western

margin of the Southern Adriatic: processes involved in transferring particulate matter to the deep basin. Mar. Geol. 375, 28–43. https://doi.org/10.1016/j.margeo.2015.09.004.
Legarreta, L., Uliana, M.A., 1998. Anatomy of Hinterland depositional sequences: upper Cretaceous fluvial strata, Neuquen basin, west-central Argentina. In: Kocurek, G. (Ed.), Relative Role of Eustacy, Climate, and Tectonism in Continental Rocks. SEPM Society for Sedimentary Geology, pp. 83–92. https://doi.org/10.2110/pec.98.59.0083.
Li, C., Wang, P., Sun, H., Zhang, J., Fan, D., Deng, B., 2002. Late Quaternary incised-valley fill of the Yangtze delta (China): its stratigraphic framework and evolution. Sediment. Geol. 152, 133–158. https://doi.org/10.1016/S0037-0738(02)00066-0.
Lin, C.-M., Zhuo, H.-C., Gao, S., 2005. Sedimentary facies and evolution in the Qiantang river incised valley, eastern China. Mar. Geol. 219, 235–259. https://doi.org/10.1016/j.margeo.2005.06.009.
Liu, J.P., Milliman, J.D., Gao, S., Cheng, P., 2004. Holocene development of the yellow river's subaqueous delta, north yellow sea. Mar. Geol. 209, 45–67. https://doi.org/10.1016/j.margeo.2004.06.009.
Manca, B.B., Kovačević, V., Gačić, M., Viezzoli, D., 2002. Dense water formation in the Southern Adriatic Sea and spreading into the Ionian Sea in the period 1997–1999. J. Mar. Syst. 33–34, 133–154. https://doi.org/10.1016/S0924-7963(02)00056-8.
Mancinelli, V., Paglia, G., Discenza, M.E., Minnillo, M., Cerrone, F., Rizzo, M., Miccadei, E., 2023. Morphotectonic features in the Middle biferno River Valley: the case of ponte liscione dam (Central Italy). Geosciences 13, 240. https://doi.org/10.3390/geosciences13080240.
Marino, G., Rohling, E.J., Sangiorgi, F., Hayes, A., Casford, J.L., Lotter, A.F., Kucera, M., Brinkhuis, H., 2009. Early and middle Holocene in the Aegean Sea: interplay between high and low latitude climate variability. Quat. Sci. Rev. 28, 3246–3262. https://doi.org/10.1016/j.quascirev.2009.08.011.
Maselli, V., Trincardi, F., 2013. Large-scale single incised valley from a small catchment basin on the western Adriatic margin (central Mediterranean Sea). Global Planet. Change 100, 245–262. https://doi.org/10.1016/j.gloplacha.2012.10.008.
Maselli, V., Trincardi, F., Asioli, A., Ceregato, A., Rizzetto, F., Taviani, M., 2014. Delta growth and river valleys: the influence of climate and sea level changes on the South Adriatic shelf (Mediterranean Sea). Quat. Sci. Rev. 99, 146–163. https://doi.org/10.1016/j.quascirev.2014.06.014.
Miall, A.D., 2013. The geology of fluvial deposits: sedimentary facies, basin analysis. And Petroleum Geology. Springer-Verlag, Berlin, p. 581.
Miserocchi, S., Langone, L., Tesi, T., 2007. Content and isotopic composition of organic carbon within a flood layer in the Po River prodelta (Adriatic Sea). Cont. Shelf Res. 27, 338–358. https://doi.org/10.1016/j.csr.2005.05.005.
Murray, J.W., 2006. Ecology and Applications of Benthic Foraminifera. Cambridge University Press.
Nijenhuis, I.A., Schenau, S.J., Van der Weijden, C.H., Hilgen, F.J., Lourens, L.J., Zachariasse, W.J., 1996. On the origin of Upper Miocene sapropelites: a case study from the Faneromeni Section, Crete (Greece). Paleoceanography 11, 633–645. https://doi.org/10.1029/96PA01963.
Orlić, M., Kuzmić, M., Pasarić, Z., 1994. Response of the Adriatic sea to the bora and sirocco forcing. Cont. Shelf Res. 14, 91–116. https://doi.org/10.1016/0278-4343(94)90007-8.
Palinkas, C.M., Nittrouer, C.A., 2006. Clinoform sedimentation along the apennine shelf, Adriatic Sea. Mar. Geol. 234, 245–260. https://doi.org/10.1016/j.margeo.2006.09.006.
Peeters, J., Busschers, F.S., Stouthamer, E., 2015. Fluvial evolution of the Rhine during the last interglacial-glacial cycle in the southern North Sea basin: a review and look forward. Quat. Int. 357, 176–188. https://doi.org/10.1016/j.quaint.2014.03.024.
Pellegrini, C., Asioli, A., Bohacs, K.M., Drexler, T.M., Feldman, H.R., Sweet, M.L., Maselli, V., Rovere, M., Gamberi, F., Valle, G.D., Trincardi, F., 2018. The Late Pleistocene Po River lowstand wedge in the Adriatic Sea: controls on architecture variability and sediment partitioning. Mar. Pet. Geol. 96, 16–50. https://doi.org/10.1016/j.marpetgeo.2018.03.002.
Pellegrini, C., Maselli, V., Cattaneo, A., Piva, A., Ceregato, A., Trincardi, F., 2015. Anatomy of a compound delta from the post-glacial transgressive record in the Adriatic Sea. Mar. Geol. 362, 43–59. https://doi.org/10.1016/j.margeo.2015.01.010.
Pellegrini, C., Maselli, V., Gamberi, F., Asioli, A., Bohacs, K.M., Drexler, T.M., Trincardi, F., 2017. How to make a 350-m-thick lowstand systems tract in 17,000 years: the Late Pleistocene Po River (Italy) lowstand wedge. Geology 45 (1), 327–330. https://doi.org/10.1130/G38848.
Pellegrini, C., Maselli, V., Trincardi, F., 2016. Pliocene–Quaternary contourite depositional system along the south-western Adriatic margin: changes in sedimentary stacking pattern and associated bottom currents. Geo Mar. Lett. 36, 67–79. https://doi.org/10.1007/s00367-015-0424-4.
Pellegrini, C., Sammartino, I., Schieber, J., Tesi, T., Paladini de Mendoza, F., Rossi, V., Chiggiato, J., Schroeder, K., Gallerani, A., Langone, L., Trincardi, F., 2024. On depositional processes governing along-strike facies variations of fine-grained deposits: unlocking the Little Ice Age subaqueous clinothems on the Adriatic shelf. Sedimentology 71 (3), 941–973. https://doi.org/10.1111/sed.13162.
Pellegrini, C., Tesi, T., Schieber, J., Bohacs, K.M., Rovere, M., Asioli, A., Nogarotto, A., Trincardi, F., 2021. Fate of terrigenous organic carbon in muddy clinothems on continental shelves revealed by stratal geometries: insight from the Adriatic sedimentary archive. Glob. Planet. Change 203, 103539. https://doi.org/10.1016/j.gloplacha.2021.103539.
Posamentier, H.W., Jervey, M.T., Vail, P.R., 1988. Eustatic controls on clastic deposition I—Conceptual framework. In: Wilgus, C.K., Hastings, B.S., Posamentier, H., Wagoner, J.V., Ross, C.A., Kendall, C.G.StC. (Eds.), Sea-Level Changes: an Integrated Approach. Society of Economic Paleontologists and Mineralogists, pp. 10–124. https://doi.org/10.2110/pec.88.01.0109.
Posamentier, H.W., Vail, P.R., 1988. Eustatic control on clastic deposition II — sequence and systems tract models. In: Wilgus, C.K., Hastings, B.S., Kendall, C.G.C., Posamentier, H.W., Ross, C.A., Van Wagoner, J.C. (Eds.), Sea-Level Changes: An Integrated Approach, 42. SEPM Special Publication, pp. 125–154.
Poulain, P.-M., 2001. Adriatic Sea surface circulation as derived from drifter data between 1990 and 1999. J. Mar. Syst. 29, 3–32. https://doi.org/10.1016/S0924-7963(01)00007-0.
Ramsey, C.B., 1995. Radiocarbon calibration and analysis of Stratigraphy: the OxCal Program. Radiocarbon 37, 425–430. https://doi.org/10.1017/S0033822200030903.
Ramsey, C.B., 2008. Deposition models for chronological records. Quat. Sci. Rev. 27, 42–60. https://doi.org/10.1016/j.quascirev.2007.01.019.
Ramsey, C.B., 2009. Bayesian analysis of radiocarbon dates. Radiocarbon 51, 337–360. https://doi.org/10.1017/S0033822200033865.
Ramsey, C.B., Lee, S., 2013. Recent and Planned Developments of the Program OxCal. Radiocarbon. https://doi.org/10.1017/S0033822200057878.
Rasmussen, T.L., Thomsen, E., Skirbekk, K., Ślubowska-Woldengen, M., Klitgaard Kristensen, D., Koç, N., 2014. Spatial and temporal distribution of Holocene temperature maxima in the northern Nordic seas: interplay of Atlantic-, Arctic- and polar water masses. Quat. Sci. Rev. 92, 280–291. https://doi.org/10.1016/j.quascirev.2013.10.034.
Ricci Lucchi, M., Fiorini, F., Luisa Colalongo, M., Vittorio Curzi, P., 2006. Late-Quaternary paleoenvironmental evolution of Lesina lagoon (southern Italy) from subsurface data. Sediment. Geol. 183, 1–13. https://doi.org/10.1016/j.sedgeo.2005.09.003.
Rodriguez, A.B., Anderson, J.B., Simms, A.R., 2005. Terrace inundation as an autocyclic mechanism for parasequence Formation: Galveston Estuary, Texas, U.S.A. J. Sediment. Res. 75 (4), 608–620. https://doi.org/10.2110/jsr.2005.050.
Rogerson, M., Cacho, I., Jimenez-Espejo, F., Reguera, M.I., Sierro, F.J., Martinez-Ruiz, F., Frigola, J., Canals, M., 2008. A dynamic explanation for the origin of the western Mediterranean organic-rich layers. Geochem. Geophys. Geosystems 9 (7). https://doi.org/10.1029/2007GC001936.
Rohling, E.J., Marino, G., Grant, K.M., 2015. Mediterranean climate and oceanography, and the periodic development of anoxic events (sapropels). Earth Sci. Rev. 143, 62–97. https://doi.org/10.1016/j.earscirev.2015.01.008.
Ronchi, L., Fontana, A., Cohen, K.M., Stouthamer, E., 2021. Late Quaternary landscape evolution of the buried incised valley of Concordia Sagittaria (Tagliamento River, NE Italy): a reconstruction of incision and transgression. Geomorphology 373, 107509. https://doi.org/10.1016/j.geomorph.2020.107509.
Rossi, V., Amorosi, A., Sarti, G., Mariotti, S., 2017. Late Quaternary multiple incised valley systems: an unusually well-preserved stratigraphic record of two interglacial valley-fill successions from the Arno Plain (northern Tuscany, Italy). Sedimentology 64 (7), 1901–1928. https://doi.org/10.1111/sed.12379.
Rossi, V., Sammartino, I., Pellegrini, C., Barbieri, G., Teodoro, C., Trincardi, F., Amorosi, A., 2024. Coupling palaeobiology and geochemistry from the Holocene of the southern Adriatic Sea (Gulf of Manfredonia, Italy): shelf facies patterns and eutrophication trends. Palaeogeogr. Palaeoclimatol. Palaeoecol. 639, 112055. https://doi.org/10.1016/j.palaeo.2024.112055.
Rossi, V., Vaiani, S.C., 2008. Benthic foraminiferal evidence of sediment supply changes and fluvial drainage reorganization in Holocene deposits of the Po Delta, Italy. Mar. Micropaleontol. 69, 106–118. https://doi.org/10.1016/j.marmicro.2008.07.001.
Rossignol-Strick, M., 1985. Mediterranean Quaternary sapropels, an immediate response of the African monsoon to variation of insolation. Palaeogeogr. Palaeoclimatol. Palaeoecol. 49, 237–263. https://doi.org/10.1016/0031-0182(85)90056-2.
Rossignol-Strick, M., Nesteroff, W., Olive, P., Vergnaud-Grazzini, C., 1982. After the deluge: mediterranean stagnation and sapropel formation. Nature 295, 105–110. https://doi.org/10.1038/295105a0.
Rosskopf, C.M., Scorpio, V., 2013. Geomorphologic map of the Biferno River valley floor system (Molise, Southern Italy). J. Maps 9, 106–114. https://doi.org/10.1080/17530350.2012.755385.
Sakai, T., Fujiwara, O., Kamataki, T., 2006. Incised-valley-fill succession affected by rapid tectonic uplifts: an example from the uppermost Pleistocene to Holocene of the Isumi River lowland, central Boso Peninsula, Japan. Sediment. Geol. 185, 21–39. https://doi.org/10.1016/j.sedgeo.2005.10.008.
Salel, T., Bruneton, H., Lefevre, D., 2016. Ostracods and environmental variability in lagoons and deltas along the north-western Mediterranean coast (Gulf of Lions, France and Ebro delta, Spain). Rev. Micropaleontol. 59 (4), 425e444. https://doi.org/10.1016/j.revmic.2016.09.001.
Sánchez Goñi, M.F., Loutre, M.F., Peyron, O., Santos, L., Duprat, J., Malaizé, B., Turon, J. L., Peypouquet, J.P., 2005. Increasing vegetation and climate gradient in Western Europe over the Last Glacial Inception (122–110 ka): data-model comparison. Earth Planet Sci. Lett. 231, 111–130. https://doi.org/10.1016/j.epsl.2004.12.010.
Sarti, G., Sarti, G., Rossi, V., Amorosi, A., 2012. Influence of Holocene stratigraphic architecture on ground surface settlements: a case study from the City of Pisa (Tuscany, Italy). Sediment. Geol. 281, 75–87. https://doi.org/10.1016/j.sedgeo.2012.08.008.
Schmiedl, G., Kuhnt, T., Ehrmann, W., Emeis, K.-C., Hamann, Y., Kotthoff, U., Dulski, P., Pross, J., 2010. Climatic forcing of eastern Mediterranean deep-water formation and benthic ecosystems during the past 22 000 years. Quat. Sci. Rev. 29, 3006–3020. https://doi.org/10.1016/j.quascirev.2010.07.002.
Scrocca, D., Tozzi, M., 1999. Tettogenesi mio-pliocenica Dell'Appennino molisano. Boll Soc Geol It 118, 255–286.
Shanley, K.W., McCabe, P.J., 1991. Predicting facies architecture through sequence stratigraphy—An example from the Kaiparowits Plateau, Utah. Geology 19 (2),

742–745. https://doi.org/10.1130/0091-7613(1991)019%3C0742:PFATSS%3E2.3.CO.
Shanley, K.W., McCabe, P.J., 1992. Alluvial Architecture in a sequence stratigraphic framework: a case history from the Upper Cretaceous of Southern Utah, USA. In: The Geological Modelling of Hydrocarbon Reservoirs and Outcrop Analogues. John Wiley & Sons, Ltd, pp. 21–55. https://doi.org/10.1002/9781444303957.ch2.
Shanley, K.W., McCabe, P.J., 1994. Perspectives on the sequence stratigraphy of continental strata: report of a working group at the 1991 NUNA conference on high-resolution sequence stratigraphy. AAPG Bull. 74, 544–568.
Simms, A.R., Anderson, J.B., Milliken, K.T., Taha, Z.P., Wellner, J.S., 2007. Geomorphology and age of the Oxygen isotope stage 2 (last lowstand) sequence boundary on the northwestern Gulf of Mexico continental shelf. In: Davies, R.J., Posamentier, H.W., Wood, L.J., Cartwright, J.A. (Eds.), Seismic Geomorphology: Applications to Hydrocarbon Exploration and Production, vol 277. Geol. Soc. Lond. Spec. Publ., pp. 29–46. https://doi.org/10.1144/GSL.SP.2007.277.01.03
Simms, A.R., Aryal, N., Miller, L., Yokoyama, Y., 2010. The incised valley of Baffin Bay, Texas: a tale of two climates. Sedimentology 57, 642–669. https://doi.org/10.1111/j.1365-3091.2009.01111.x.
Sloss, C.R., Jones, B.G., Switzer, A.D., Nichol, S., Clement, A.J.H., Nicholas, A.W., 2010. The Holocene infill of Lake Conjola, a narrow incised valley system on the southeast coast of Australia. Quat. Int. 221, 23–35. https://doi.org/10.1016/j.quaint.2009.06.027.
Sømme, T.O., Helland-Hansen, W., Granjeon, D., 2009. Impact of eustatic amplitude variations on shelf morphology, sediment dispersal, and sequence stratigraphic interpretation: icehouse versus greenhouse systems. Geology 37 (7), 587–590. https://doi.org/10.1130/G25511A.1.
Sømme, T.O., Piper, D.J.W., Deptuck, M.E., Helland-Hansen, W., 2011. Linking onshore-offshore sediment dispersal in the Golo source-to-sink System (Corsica, France) during the late Quaternary. J. Sediment. Res. 81 (2), 118–137. https://doi.org/10.2110/jsr.2011.11.
Soil Survey Staff, 1999. Soil taxonomy—A basic system of soil classification for making and interpreting soil surveys. Agricultural Handbook 436, Natural Resources Conservation Service, second ed. USDA, Washington DC, USA, p. 869. https://doi.org/10.1111/j.1475-2743.2001.tb00008.x.
Spötl, C., Nicolussi, K., Patzelt, G., Boch, R., 2010. Humid climate during deposition of sapropel 1 in the Mediterranean Sea: assessing the influence on the Alps. Glob. Planet. Change 71, 242–248. https://doi.org/10.1016/j.gloplacha.2009.10.003.
Storms, J.E.A., Weltje, G.J., Terra, G.J., Cattaneo, A., Trincardi, F., 2008. Coastal dynamics under conditions of rapid sea-level rise: late Pleistocene to early Holocene evolution of barrier–lagoon systems on the northern Adriatic shelf (Italy). Quat. Sci. Rev. 27, 1107–1123. https://doi.org/10.1016/j.quascirev.2008.02.009.
Strong, N., Paola, C., 2006. Fluvial landscape sand stratigraphy in a flume. Sediment. Rec. 4, 3–7.
Strong, N., Paola, C., 2008. Valleys that never were: time surfaces versus stratigraphic surfaces. J. Sed. Res 78, 579–593. https://doi.org/10.2110/jsr.2008.059.
Sweet, M.L., 2020. Controls on the grain size of sediment routed to deep water: insights from Quaternary systems. Res. Ins. 2 (4).
Tachikawa, K., Vidal, L., Cornuault, M., Garcia, M., Pothin, A., Sonzogni, C., Bard, E., Menot, G., Revel, M., 2015. Eastern Mediterranean Sea circulation inferred from the conditions of S1 sapropel deposition. Clim. Past 11, 855–867. https://doi.org/10.5194/cp-11-855-2015.
Tanabe, S., Ishihara, Y., 2021. Formation of undulating topography and gravel beds at the bases of incised valleys: last Glacial Maximum examples beneath the lowlands facing Tokyo Bay. Prog. Earth Planet. Sci. 8, 20. https://doi.org/10.1186/s40645-021-00411-0.
Tanabe, S., Ishihara, Y., Nishiyama, K., Sato, Y., 2026. Tectonic control on incised-valley geometry: late Pleistocene examples along the longest active fault in Japan. Geomorphology 498, 110207. https://doi.org/10.1016/j.geomorph.2026.110207.
Tanabe, S., Nakanishi, T., Ishihara, Y., Nakashima, R., 2015. Millennial-scale stratigraphy of a tide-dominated incised valley during the last 14 kyr: spatial and quantitative reconstruction in the Tokyo Lowland, central Japan. Sedimentology 62 (7), 1837–1872. https://doi.org/10.1111/sed.12204.
Tanabe, S., Nakanishi, T., Matsushima, H., Hong, W., 2013. Sediment accumulation patterns in a tectonically subsiding incised valley: insight from the Echigo Plain, central Japan. Mar. Geol. 336, 33–43. https://doi.org/10.1016/j.margeo.2012.11.006.
Tanabe, S., Saito, Y., Lan Vu, Q., Hanebuth, T.J.J., Lan Ngo, Q., Kitamura, A., 2006. Holocene evolution of the Song Hong (Red River) delta system, northern Vietnam. Sediment. Geol. 187, 29–61. https://doi.org/10.1016/j.sedgeo.2005.12.004.
Tesi, T., Asioli, A., Massara, E.P., Montagna, P., Pellegrini, C., Nogarotto, A., Cipriani, A., Piva, A., Muschitiello, F., Rovere, M., Viaggi, P., Trincardi, F., 2024. Abrupt and persistent shutdown of the thermohaline forcing during MIS5e in the Adriatic Sea: insights from shallow-water sapropel sediments. Quat. Sci. Adv. 13, 100134. https://doi.org/10.1016/j.qsa.2023.100134.
Tesi, T., Asioli, A., Minisini, D., Maselli, V., Dalla Valle, G., Gamberi, F., Langone, L., Cattaneo, A., Montagna, P., Trincardi, F., 2017. Large-scale response of the Eastern Mediterranean thermohaline circulation to African monsoon intensification during sapropel S1 formation. Quat. Sci. Rev. 159, 139–154. https://doi.org/10.1016/j.quascirev.2017.01.020.
Tesi, T., Miserocchi, S., Goñi, M.A., Langone, L., Boldrin, A., Turchetto, M., 2007. Organic matter origin and distribution in suspended particulate materials and surficial sediments from the western Adriatic Sea (Italy). Estuar. Coast Shelf Sci. 73, 431–446. https://doi.org/10.1016/j.ecss.2007.02.008.
Thomas, M.A., Anderson, J.B., 1994. Sea-Level controls on the facies Architecture of the Trinity/Sabine incised-valley System, Texas Continental Shelf. In: Dalrymple, R.W., Boyd, R., Zaitlin, B.A. (Eds.), Incised-Valley Systems: Origin and Sedimentary Sequences, vol. 51. SEPM Society for Sedimentary Geology, pp. 63–82. https://doi.org/10.2110/pec.94.12.0063.
Toucanne, S., Minto'o, C.M.A., Fontanier, C., Bassetti, M.A., Jorry, S.J., Jouet, G., 2015. Tracking rainfall in the northern Mediterranean borderlands during sapropel deposition. Quat. Sci. Rev. 129, 178–195. https://doi.org/10.1016/j.quascirev.2015.10.016.
Trincardi, F., Correggiari, A., Roveri, M., 1994. Late Quaternary transgressive erosion and deposition in a modern epicontinental shelf: the Adriatic semienclosed basin. Geo Mar. Lett. 14, 41–51. https://doi.org/10.1007/BF01204470.
Vacchi, M., Marriner, N., Morhange, C., Spada, G., Fontana, A., Rovere, A., 2016. Earth Science Reviews Multiproxy assessment of Holocene relative sea-level changes in the western Mediterranean: Sea-level variability and improvements in the definition of the isostatic signal. Earth Sci. Rev. 155, 172–197. https://doi.org/10.1016/j.
Van Wagoner, J.C.V., Mitchum, R.M., Campion, K.M., Rahmanian, V.D., 1990. Siliciclastic sequence stratigraphy in well logs, cores, and outcrops: concepts for high-resolution correlation of time and facies. American Association of petroleum geologists methods. Explor. Spec. 7, 55.
Van Wagoner, J.C.V., Posamentier, H.W., Mitchum, R.M., Vail, P.R., Sarg, J.F., Loutit, T.S., Hardenbol, J., 1988. An overview of the fundamentals of sequence stratigraphy and key definitions. In: Wilgus, C.K., Hastings, B.S., Posamentier, H., Wagoner, J.V., Ross, C.A., Kendall, C.G.StC. (Eds.), Sea-Level Changes: an Integrated Approach, vol. 42. Society of Economic Paleontologists and Mineralogists, pp. 39–45. https://doi.org/10.2110/pec.88.01.0039.
Wagner, B., Vogel, H., Francke, A., Friedrich, T., Donders, T., Lacey, J.H., Leng, M.J., Regattieri, E., Sadori, L., Wilke, T., Zanchetta, G., 2019. Mediterranean winter rainfall in phase with African monsoons during the past 1.36 million years. Nature 573, 256–260. https://doi.org/10.1038/s41586-019-1529-0.
Wang, R., Colombera, L., Mountney, N.P., 2019. Geological controls on the geometry of incised-valley fills: insights from a global dataset of late-quaternary examples. Sedimentology 66, 2134–2168. https://doi.org/10.1111/sed.12596.
Weldeab, S., Menke, V., Schmiedl, G., 2014. The pace of East African monsoon evolution during the Holocene. Geophys. Res. Lett. 41, 1724–1732. https://doi.org/10.1002/2014GL059361.
Wilson, A.M., Osborne, A., White, S.M., 2024. Large-scale groundwater flow and sedimentary diagenesis in continental shelves influence marine chemical budgets. Nat. Commun. 15, 1143. https://doi.org/10.1038/s41467-024-44919-7.
Wright, V.P., Marriott, S.B., 1993. The sequence stratigraphy of fluvial depositional systems: the role of floodplain sediment storage. Sediment. Geol. 86, 203–210. https://doi.org/10.1016/0037-0738(93)90022-W.
Zaitlin, B., Dalrymple, R., Boyd, R., 1994. The stratigraphic organization of incised valley systems associated with relative sea-level change. In: Dalrymple, R.W., Boyd, R., Zaitlin, B.A. (Eds.), Incised-Valley Systems: Origin and Sedimentary Sequences, vol. 51. SEPM Special Publication, pp. 45–60. https://doi.org/10.2110/pec.94.12.0045.
Zanchetta, G., Drysdale, R.N., Hellstrom, J.C., Fallick, A.E., Isola, I., Gagan, M.K., Pareschi, M.T., 2007. Enhanced rainfall in the Western Mediterranean during deposition of sapropel S1: stalagmite evidence from Corchia cave (Central Italy). Quat. Sci. Rev. 26, 279–286. https://doi.org/10.1016/j.quascirev.2006.12.003.
Zecchin, M., Donda, F., Forlin, E., 2017. Genesis of the Northern Adriatic Sea (Northern Italy) since early Pliocene. Mar. Pet. Geol. 79, 108–130. https://doi.org/10.1016/j.marpetgeo.2016.11.009.
Zhang, Y., Li, Ziying, Qin, M., Bao, Z., Li, Zhixing, Yi, L., Li, G., 2021. Sedimentology and stratigraphy sequence of the north of Saudi Arabia: implications for the evolution of the Neo-Tethys in the Late Cretaceous. Geol. J. 56, 1510–1530. https://doi.org/10.1002/gj.4013.